INTERNATIONAL JOURNAL FOR NUMERICAL METHODS IN ENGINEERING
Int. J. Numer. Meth. Engng 2014; **99**:129–156
Published online 30 April 2014 in Wiley Online Library (wileyonlinelibrary.com). DOI: 10.1002/nme.4676

A level set approach for topology optimization with local stress constraints

Hélio Emmendoerfer Jr. and Eduardo Alberto Fancello*,†

Department of Mechanical Engineering, Federal University of Santa Catarina, Campus Universitário - Trindade, 88040-900, Florianópolis, SC, Brazil

SUMMARY

The purpose of this work is to present a level set-based approach for the structural topology optimization problem of mass minimization submitted to local stress constraints. The main contributions are three-fold. First, the inclusion of local stress constraints by means of an augmented Lagrangian approach within the level set context. Second, the proposition of a constraint procedure that accounts for a continuous activation/deactivation of a finite number of local stress constraints during the optimization sequence. Finally, the proposition of a logarithmic scaling of the level set normal velocity as an additional regularization technique in order to improve the minimization sequence. A set of benchmark tests in two dimensions achieving successful numerical results assesses the good behavior of the proposed method. In these examples, it is verified that the algorithm is able to identify stress concentrations and drive the design to a feasible local minimum. Copyright © 2014 John Wiley & Sons, Ltd.

Received 13 December 2013; Revised 26 February 2014; Accepted 21 March 2014

KEY WORDS: topology optimization; level sets; stress constraints; augmented Lagrangian; topology design; structural optimization

1. INTRODUCTION

The topological optimization of continuous structures has been an area of research of important recognition in the last decades. While most of the literature focuses on the problem of maximum stiffness (compliance problem) due to its own mathematical characteristics, in the last years, attention has regained to the structural problem related to minimizing of mass subject to local stress constraints. However, this problem possesses some difficulties. One being the difficulty introduced by local constraints, that is, stress levels at every material point must be constrained according to failure criteria. Another is related to the so-called stress singularity phenomenon.

The study in [1] is, to the author's knowledge, the first work addressing topology optimization problems with stress constraints in the context of continuum structures using the concept of intermediate artificial material Solid Isotropic Microstructure with Penalization (SIMP). This article emphasizes the difficulty of the treatment of the stress constraint and the singularity phenomenon. The work in [2] uses the same SIMP approach and a proposal of solution based on the augmented Lagrangian technique. This approach is extended to multiple loading conditions [3] and contact boundary conditions [4]. On the other hand, the work in [5] also extended the homogenization method to treat problems involving stress but to objective functions corresponding to minimum stress design subject to volume constraint. Also using SIMP concepts, the qp-approach [6] was tested for topology optimization problems where minimum compliance is the objective function and local constraints have been locally imposed on von Mises stress of each element [7].

*Correspondence to: Eduardo Alberto Fancello, Department of Mechanical Engineering, Federal University of Santa Catarina, Campus Universitário - Trindade, 88040-900, Florianópolis, SC, Brazil.
†E-mail: fancello@grante.ufsc.br; helio.e.j@posgrad.ufsc.br

Some works such as [2, 4, 8] and others calculate the stress in the center of each element by generating optimization problems numerically challenging because of the large number of local stress constraints. On the other hand, several works [9–12] do not treat constraints as a local measure but as a global approximation of the local stress constraints such as the p-norm or the Kreisselmeier–Steinhauser function. However, it is known that using a global stress measure decreases the computational expense but usually provides poor local control over the stress distribution. With the aim for overcoming this undesirable side effect, some works have developed some criteria to improve the use of global approximation. For instance, the work in [13] proposes the use of the superconvergent patch recovery schemes to evaluate the stress field leading to a more reliable evaluation of the global constraint. The approach in [14] groups elements in blocks or groups of elements (block aggregated constraints approach) and thus produce a single stress constraint per block using the Kreisselmeier–Steinhauser function. Similarly, the study in [15] uses the p-norm to compute the normalized global stress measure of a set of elements belonging to regions within the domain. Recently, the work in [12] uses a clustering technique, where stresses for several stress evaluation points are clustered into groups using a modified p-norm.

A different proposal is based on the concept of topological derivative to solve local stress constraint problems with different failure criteria, presenting very satisfactory results [8, 16].

In this study, the problem of minimizing the mass of a body subject to local stress constraints is addressed on the basis of a level set approach. The researchers in [17] are among the first to introduce the level set method in structural topology optimization problems. On the other hand, the papers in [18] and [19] relate the information provided by shape sensitivity analysis with the movement of the level set. It is well known however that these conventional level set methods present some unfavourable numerical issues. Because of this, alternative level set-based techniques have been developed for shape and topology optimization [20–26]. For a survey on the level set method, the reader may refer to [27] and [28], and for a very thorough review regarding the use of different level set techniques for structural topology optimization, see [29].

One of the first studies using the level set method for problems involving stresses is found in [30], where a norm of the stress over the domain is used as objective function. In [31] is presented an extension of that work to irregular domains and non-uniform meshes. The information of the shape sensitivities of the von Mises stress function is isoparametricly mapped for a uniform Cartesian mesh in which the equation of Hamilton–Jacobi is solved. A different approach linking the level set method and stress constraints is due to [32] dealing with stress concentration minimization of 2D fillets based on the level set description and the extended finite element method (X-FEM).

Early works using the level set method to deal with minimization of mass and stress constraints were presented at conferences, for example, in [11], where the stress constraints are aggregated in a single equivalent global constraint, and in [33], where regularized formulations for stress-related topology optimization are proposed [34]. The study in [35] minimizes a global measure of von Mises stress subject to a constraint of material volume. The level set controls the domain, and the background mesh is constantly updated in order to follow the moving boundaries. The work in [36] uses constraint aggregation techniques to deal with the local nature of the stress dividing the domain in sub-domains called group constraints. The article in [37] presents a level set/X-FEM approach to reduce the volume of a structure proposing a single stress constraint (called shape equilibrium constraint function) for the optimization problem, relieving the computational expenses.

The study in [38] presents an algorithm for stress-constrained problems that relies on tracking a level set defined via the topological derivative. Also, Zhang *et al*. [39] used the level set method for designing stiff structures with less stress concentrations.

This present work deals with the problem of mass minimization subject to von Mises-based stress constraints imposed locally in a finite number of sample points uniformly distributed along the domain. The number of these sample points should be enough to identify all possible stress peaks that may occur during the optimization process. The formulation is based on the level set approach to control the domain, while the augmented Lagrangian mathematical programming technique is used to account for the stress constraints in a form similar to that proposed in [2]. This technique is able to automatically perform the appropriate selection of the relevant (active) stress constraints among the domain. The main objective is to create an efficient algorithm capable of identifying

DOI: 10.1002/nme

stress concentration regions and change the topology to a feasible local minimum. Being the stress constraint the main focus of the present work, the implementation of the level set updating was here restricted, as a first attempt, to the conventional upwind schemes shown in [27, 28].

In order to obtain a sequence of ideas for a better understanding of the procedure, the paper is organized as follows. Section 2 states briefly the basic formulation of the problem, presents the definition of the stress constraint, and states the augmented Lagrangian formulation using the level set concepts. Section 3 shows the analytical sensitivity analysis of the final Lagrangian functional and its relation with velocity field of the level set methods. Section 4 presents the optimization algorithm proposed and some operational details. Section 5 is dedicated to the numerical results and discussions about the proposed approach. Some conclusions are stated in Section 6. Finally, the Appendix shows details about the derivatives of the stress constraints based on a failure criterion.

2. FORMULATION OF THE PROBLEM

2.1. Basic statement

Let Ω be an open domain in $\mathbb{R}^n$ $(n = 2, 3)$ occupied by a linear elastic isotropic body $\mathcal{B}$ with a smooth boundary $\partial\Omega$ split in three non-overlapping regions

$$\partial\Omega = \Gamma_D \cup \Gamma_H \cup \Gamma_N. \tag{1}$$

Dirichlet boundary conditions are applied in Γ_D, while Γ_H is submitted to homogeneous Neumann conditions. Non-zero surface tractions $\boldsymbol{\tau}$ act on Γ_N. It is assumed that Γ_H may change during the optimization procedure, while Γ_D and Γ_N remain fixed. It is also assumed that all the admissible configurations Ω are defined within a fixed background domain D (Figure 1).

The principle of virtual work states that the body $\mathcal{B}$ achieves equilibrium when the displacement field $\mathbf{u} \in U$ satisfies the expression

$$a(\mathbf{u}, \mathbf{v}) = l(\mathbf{v}) \quad \forall \mathbf{v} \in V, \tag{2}$$

$$a(\mathbf{u}, \mathbf{v}) = \int_\Omega \mathbf{C}\boldsymbol{\varepsilon}(\mathbf{u}) \cdot \boldsymbol{\varepsilon}(\mathbf{v})\, d\Omega\,, \tag{3}$$

$$l(\mathbf{v}) = \int_{\Gamma_N} \boldsymbol{\tau} \cdot \mathbf{v}\, d\,\partial\Omega, \tag{4}$$

where U and V denote the sets of kinematically admissible displacements and admissible variations, respectively. The bilinear operator $a(\cdot,\cdot)$ represents the virtual work of internal forces, and $l(\cdot)$ is a linear form accounting for the virtual work of external surface forces. $\boldsymbol{\varepsilon}(\mathbf{u}) = \nabla^s\mathbf{u}$ is the linear strain tensor, and $\mathbf{C}$ is the isotropic elasticity tensor. For simplicity reasons, the problem in which

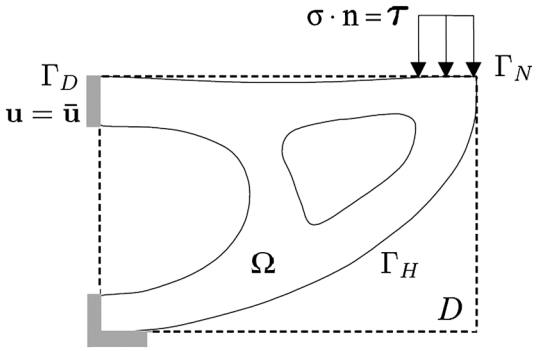

Figure 1. Geometric definitions of a domain composed of solid and voids.

DOI: 10.1002/nme

the loading is design dependent is not addressed here (see, for example, [40]), and therefore, no body forces are considered in (4).

The problem of minimum mass with local stress (failure) constraints can be stated as

Problem P_1*:*

$$\begin{aligned} \min_{\Omega} \quad & m(\mathbf{u}) = \int_{\Omega} \rho d\Omega, \\ \text{subject to:} \quad & \begin{cases} a_{\Omega}(\mathbf{u},\mathbf{v}) - l_{\Omega}(\mathbf{v}) = 0, & \forall \mathbf{v} \in V, \\ g(\mathbf{u}) \leqslant 0, & \forall \mathbf{x} \in \Omega\ , \end{cases} \end{aligned} \tag{5}$$

where ρ is the material density and $g(\mathbf{u})$ is a stress constraint that must be satisfied almost everywhere in Ω. This approach, however, is too general for practical optimization purposes, and it will be rewritten in the present work as a moving boundary problem controlled by a level set function.

2.2. *Level set-based formulation*

The level set approach in topology optimization consists of relating the boundary $\partial\Omega$ with the zero-valued level set of a function $\phi : D \to \mathbb{R}$:

$$\phi(\mathbf{x}) > 0 \quad \forall \mathbf{x} \in \Omega, \tag{6}$$

$$\phi(\mathbf{x}) = 0 \quad \forall \mathbf{x} \in \partial\Omega, \tag{7}$$

$$\phi(\mathbf{x}) < 0 \quad \forall \mathbf{x} \in D \backslash (\Omega \cup \partial\Omega). \tag{8}$$

Expressions (6)–(8) define the region in D occupied by Ω, by the boundary $\partial\Omega$, and by the complement $D\backslash(\Omega \cup \partial\Omega)$. Variations of ϕ modify the corresponding level sets and consequently the position of the boundary $\partial\Omega$ [27, 41]. Using the Heaviside function

$$H(\phi(\mathbf{x})) = \begin{cases} 1\ , \text{ if } \phi(\mathbf{x}) \geqslant 0, \\ 0\ , \text{ if } \phi(\mathbf{x}) < 0, \end{cases} \tag{9}$$

it is possible to formulate an alternative expression for Problem P_1 as follows:

Problem P_2:

$$\begin{aligned} \min_{\phi} \quad & m_{\phi}(\mathbf{u}) = \int_{D} \rho(\phi) dD, \\ \text{subject to:} \quad & \begin{cases} a_{\phi}(\mathbf{u},\mathbf{v}) = l_{\phi}(\mathbf{v}), & \forall \mathbf{v} \in V, \\ H(\phi) g(\mathbf{u}) \leqslant 0, & \forall \mathbf{x} \in D, \end{cases} \end{aligned} \tag{10}$$

where

$$\rho(\phi) = H(\phi)\rho_1 + (1 - H(\phi))\rho_2, \tag{11}$$

$$a_{\phi}(\mathbf{u},\mathbf{v}) = \int_{D} \mathbf{C}(\phi)\boldsymbol{\varepsilon}(\mathbf{u}) \cdot \boldsymbol{\varepsilon}(\mathbf{v}) dD, \tag{12}$$

$$l_{\phi}(\mathbf{v}) = \int_{\Gamma_N} \boldsymbol{\tau} \cdot \mathbf{v} d\partial\Omega, \tag{13}$$

$$\mathbf{C}(\phi) = H(\phi)\mathbf{C}_1 + (1 - H(\phi))\mathbf{C}_2. \tag{14}$$

DOI: 10.1002/nme

Equations (11) and (14) define the fields ρ and $\mathbf{C}$ being dependent of two material phases $(\rho_1, \mathbf{C}_1)$ and $(\rho_2, \mathbf{C}_2)$. It is assumed that the material 1 occupies the domain Ω while the material 2 is occupied by the complement $D\backslash(\Omega\cup\partial\Omega)$. In the present case, the properties of material 2 are assumed to have null values or, by operational reasons during the solution of the equilibrium equations, values significantly lower than those of material 1, that is, $\rho_2 << \rho_1$ and $\|\mathbf{C}_2\| << \|\mathbf{C}_1\|$.

The use of the Heaviside function within the integral expressions has consequences that are worthy of careful discussion. One of the advantages of this approach is the possibility of using a fixed mesh over which the domain Ω evolves guided by the function ϕ. Within this context, the frontier $\partial\Omega$ does not coincide in general with the elements boundaries, and therefore, many of them are cut by $\partial\Omega$ in two parts belonging to materials 1 and 2, respectively. A possible way of getting rid of this ambiguous situation is to conform the discretization to the crossing boundary by means of remeshing [35] or, for example, by using discontinuous functions of X-FEM type [32, 37]. These options, however, introduce extra computational effort and will not be followed in the present work. Consequently, two technical questions must be addressed. The first one is related to the computation of the integral term $a_\phi(\mathbf{u}, \mathbf{v})$ and particularly on those elements cut by $\partial\Omega$. The second one is the definition of the stress constraint in those cut elements. These two questions are discussed in the following items.

2.3. State equations

The finite element counterpart of expression (12) involves the integration over all elements, some of which are crossed by the boundary $\partial\Omega$. In these cases, the material property distribution is discontinuous within the element (expression (14)), and the integration operation must take this fact into account. A possible approximation of it is using a representative constant value for $\mathbf{C}$ that accounts for the volume fraction of each material within the element:

$$\begin{aligned} a_\phi(\mathbf{u}, \mathbf{v}) &= \sum\nolimits_{e=1}^{Nel} \int_{D_e} \mathbf{C}(\phi)\boldsymbol{\varepsilon}(\mathbf{u}) \cdot \boldsymbol{\varepsilon}(\mathbf{v}) dD, \\ &\approx \sum\nolimits_{e=1}^{Nel} \int_{D_e} \mathbf{C}^e \boldsymbol{\varepsilon}(\mathbf{u}) \cdot \boldsymbol{\varepsilon}(\mathbf{v}) dD, \end{aligned} \tag{15}$$

where

$$\mathbf{C}^e = a^e \mathbf{C}_1 + (1 - a^e)\mathbf{C}_2, \tag{16}$$

$$a^e = \frac{\int_{D_e} H(\phi) dD}{\int_{D_e} dD}. \tag{17}$$

This approximation is indeed analogous to the common use of the ersatz or intermediate material. However, it must be emphasized that in this case, there is no microstructure involved but an element partially covered by Ω. Because of this, the relationship between $\mathbf{C}$ and area fraction was assumed to be linear.

2.4. Stress constraint definition

In the way Problem 2 is presented in (10), the stress constraint $g(\sigma(\mathbf{u}))$ must be satisfied almost everywhere in D. Nevertheless, this condition is inevitably transferred sometime during discretization to a finite number of constraints commonly associated to the integration points or nodes of the mesh. Being aware of this fact, it has been chosen here to substitute, at formulation level, the continuum constraint g in (5) by a finite number of stress constraints g_r defined at sample points $\mathbf{x}_r \in D$, $r = 1, \ldots, N_r$ (it is expected that the quantity and distribution of these sample points is linked with the discretization in the sense that provides a consistent approximation of the continuum case). It must be noted that just those points $\mathbf{x}_r$ belonging to Ω must be effectively considered within

DOI: 10.1002/nme

the constraint set. Thus, in order to avoid the problems associated to the discontinuous inclusion–exclusion of constraints as long as the boundary of Ω pass over a sample point, a regularization scheme is here proposed. Aiming at this, let $\boldsymbol{\varepsilon}_r(\mathbf{u})$ be the strain evaluated at $\mathbf{x}_r \in D$ and $\boldsymbol{\sigma}_r$ the stress tensor defined by

$$\boldsymbol{\sigma}_r := \mathbf{C}_1 \boldsymbol{\varepsilon}_r(\mathbf{u}). \tag{18}$$

The classical von Mises stress criterion can be written as

$$\frac{\sigma_r^{vM}}{\sigma_{adm}} - 1 \leqslant 0\,, \quad \sigma_r^{vM} = \sqrt{\frac{3}{2}\mathbf{s}_r \cdot \mathbf{s}_r}\,, \quad \mathbf{s}_r = \mathrm{dev}(\boldsymbol{\sigma}_r), \tag{19}$$

where σ_{adm} is the yield stress. Let $H_r(\phi)$ also be a function that computes the volumetric (area) fraction of material 1 contained in a neighborhood Ω_r of $\mathbf{x}(r)$ as follows:

$$H_r(\phi) = \frac{1}{a_r}\int_D I_r(\mathbf{x}) H(\phi) dD, \tag{20}$$

in which

$$I_r(\mathbf{x}) = \begin{cases} 1\,, & \text{if } \mathbf{x} \in \Omega_r, \\ 0\,, & \text{if } \mathbf{x} \notin \Omega_r, \end{cases} \quad \text{and} \quad a_r = \int_D I_r(\mathbf{x}) dD, \tag{21}$$

are the indicator function and the physics volume (area) of the neighborhood Ω_r, respectively. Figure 2 shows a schematic representation of these functions. In this way, $H_r(\phi)$ varies continuously between 0 and 1 as long as Ω covers Ω_r.

Using the definitions earlier, our purpose is to define a stress constraint g_r that follows the continuous variation of $H_r(\phi)$ during the movement of $\partial\Omega$ in such a way that the stress at $\mathbf{x}_r$ be

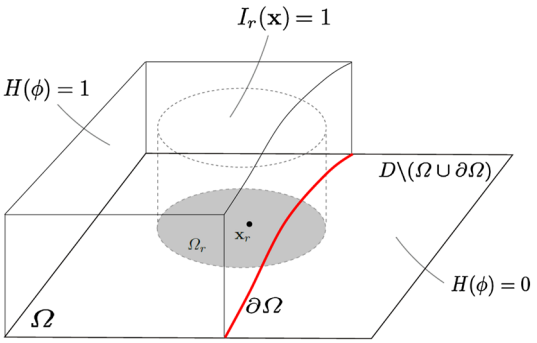

Figure 2. Representation of the indicator function $I_r(\mathbf{x})$ and Heaviside function $H(\phi)$ at a sample point $\mathbf{x}_r$ with neighborhood Ω_r.

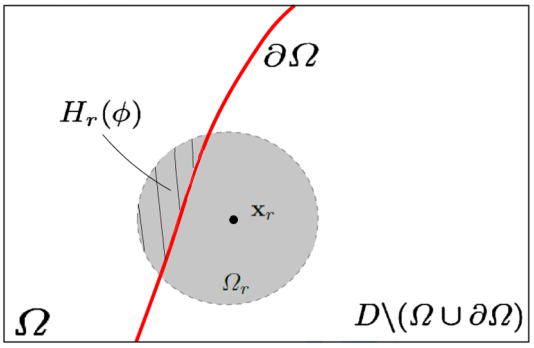

Figure 3. Sample point $\mathbf{x}_r$ and its neighborhood Ω_r being intercepted by the border $\partial\Omega$. In this case, $\mathbf{x}_r \notin \Omega$, but the stress constraint may become active because $\Omega \cap \Omega_r \neq \emptyset$, that is, $H_r(\phi) \neq 0$.

DOI: 10.1002/nme

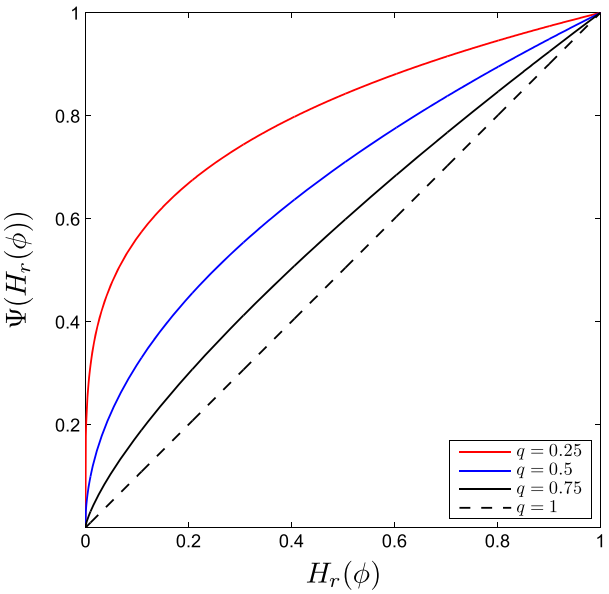

Figure 4. Function $\Psi(H_r(\phi))$ for different values of q.

significant whenever $\Omega \cap \Omega_r \neq \emptyset$. Figure 3 shows a sample point $\mathbf{x}_r$ whose corresponding constraint g_r might become active even though this point is outside Ω. A possible expression to accomplish this task is

$$g_r(\mathbf{u}, \phi) = \Psi(H_r(\phi)) \frac{\sigma_r^{vM}}{\sigma_{adm}} - 1 \leqslant 0, \tag{22}$$

with

$$\Psi(H_r(\phi)) = H_r(\phi)^q. \tag{23}$$

The purpose of function Ψ is enhancing the stress value of a point whose area fraction is $0 < H_r(\phi) < 1$. Figure 4 shows the behavior of $\Psi(H_r(\phi))$ for different values of $q \in (0, 1]$. It is clear that (23) represents a regularized version of the discontinuous $0 - 1$ function.

It is important to remark that regardless the point $\mathbf{x}_r$ is inside or outside the body, the corresponding stress $\boldsymbol{\sigma}_r$ is always calculated by Equation (18) and the stress constraint by Equation (22). The variable that turns this stress significant or not is the area fraction $H_r(\phi)$. The use of the function Ψ is conceptually related to the singularity stress phenomenon and therefore to the qp-approach [6] and more indirectly, to the ϵ-relaxation [42] used in [1]. Nevertheless, it is important to remark once again that, different from these last mentioned works, the present approach involves no intermediate material. Expression (22) should then be interpreted as a regularized way to effectively consider the stress of a sample point as long as the boundary Γ_H moves in D.

On the basis of all these considerations, the minimization problem is reformulated as follows:

Problem P_3:

$$\begin{aligned} \min_{\phi} \quad & m_\phi(\mathbf{u}) = \int_D \rho(\phi) dD, \\ \text{subject to:} \quad & \begin{cases} a_\phi(\mathbf{u}, \mathbf{v}) = l_\phi(\mathbf{v}), & \forall \mathbf{v} \in V, \\ g_r(\mathbf{u}, \phi) \leqslant 0, & r = 1, \ldots, N_r \end{cases} \end{aligned} \tag{24}$$

where $g_r(\mathbf{u}, \phi)$ is given by (22) and N_r is the total number of sample points $\mathbf{x}_r$ in D.

DOI: 10.1002/nme

2.5. Augmented Lagrangian-based formulation

Following the conventional augmented Lagrangian approach [43, 44], the stress constraints of Problem P_3 are raised up to the objective function by means of a penalization comprised by a linear and quadratic term. The main idea consists of defining a sequence $\{\alpha_r^k\}$, $k = 1, 2, \ldots$ converging to the Lagrange multipliers α_r that satisfy the necessary optimality conditions of P_3. The problem then takes the following new expression:

Problem P_4: for given values of penalization factor c^k and Lagrange multipliers α_r^k, solve the minimization

$$\begin{aligned} &\min_{\phi} \quad J^k(\phi), \\ &J^k(\phi) = \int_D \rho(\phi) dD + \sum_{r=1}^{N_r} \left\{ \alpha_r^k h_r(\mathbf{u}, \phi) + \frac{c^k}{2} [h_r(\mathbf{u}, \phi)]^2 \right\}, \end{aligned} \tag{25}$$

$$a_\phi(\mathbf{u}, \mathbf{v}) = l_\phi(\mathbf{v}), \quad \forall \mathbf{v} \in V, \tag{26}$$

where $\mathbf{u}$ is the solution of (26) and $h_r(\mathbf{u}, \phi)$ is a function of the r-th stress constraint given by [43, 44]:

$$h_r(\mathbf{u}, \phi) = \max \left\{ g_r(\mathbf{u}, \phi); -\frac{\alpha_r^k}{c^k} \right\}. \tag{27}$$

Once the minimum is achieved (or after a conveniently specified number of iterations), verify the condition:

$$\left| \alpha_r^k g_r^k \right| < \varepsilon, \tag{28}$$

where ε is a small tolerance. If (28) is not satisfied, update the Lagrange multipliers and penalization factor:

$$\begin{aligned} \alpha_r^{k+1} &= \max \left\{ \alpha_r^k + c^k g_r^k; 0 \right\}, \\ c^{k+1} &= \beta c^k, \quad \beta > 1, \quad 0 < c^k < c_{\max}, \quad \forall k \in N. \end{aligned} \tag{29}$$

Let $k = k + 1$ and restart the process.

3. OPTIMIZATION BY MOVING THE LEVEL SET

A classic way of modifying ϕ in (25) in order to obtain a minimization sequence consists of solving the time differential equation of Hamilton–Jacobi

$$\frac{\partial \phi(\mathbf{x}(t), t)}{\partial t} - \mathbf{v}(\mathbf{x}(t)) \cdot \nabla \phi(\mathbf{x}(t), t) = 0, \tag{30}$$

where $\mathbf{v}(\mathbf{x}(t))$ is the velocity for every point $\mathbf{x}(t)$ on the boundary. Because $\mathbf{n} = -\nabla\phi / \|\nabla\phi\|$, we can rewrite the equation earlier as

$$\frac{\partial \phi(\mathbf{x}(t), t)}{\partial t} - v_n(\mathbf{x}(t)) \|\nabla \phi(\mathbf{x}(t), t)\| = 0, \tag{31}$$

where $v_n = \mathbf{v} \cdot \mathbf{n}$ is the velocity normal to the boundary $\partial\Omega$, that is, for all $\mathbf{x}(t)$ with $\phi(\mathbf{x}(t)) = 0$. Equation (31) is known as the level set equation [27, 28, 41]. A key issue in this equation is the choice of a proper field v_n that guarantees that for a sufficiently small time interval Δt, the new field ϕ decreases $J^k(\phi)$. Following the same arguments used by [19] and [18], it is concluded that the derivative $\frac{dJ}{d\phi}[\delta\phi]$ provides this information. The next subsection describes the calculus of this derivative as well as its convenient postprocessing to obtain an efficient field v_n.

DOI: 10.1002/nme

3.1. Sensitivity analyisis

The total derivative $\frac{dJ}{d\phi}[\delta\phi]$ must be calculated considering the satisfaction of the state equation. To this purpose, the Lagrangian function £ is defined as follows:

$$\begin{aligned}\pounds(\phi,\mathbf{u},\boldsymbol{\lambda}) = \int_D \rho(\phi)dD + \sum_{r=1}^{Nr}\left\{\alpha_r h_r(\mathbf{u},\phi) + \frac{c}{2}\left[h_r(\mathbf{u},\phi)\right]^2\right\} \\ + a_\phi(\mathbf{u},\boldsymbol{\lambda}) - l_\phi(\boldsymbol{\lambda}) \quad \forall \mathbf{u},\boldsymbol{\lambda} \in V,\end{aligned} \tag{32}$$

being $\boldsymbol{\lambda} \in V$ a Lagrangian multiplier. The total variation of £ with respect to $\phi, \mathbf{u}, \boldsymbol{\lambda}$ is

$$\delta\pounds(\phi,\mathbf{u},\boldsymbol{\lambda}) = \frac{\partial\pounds}{\partial\phi}[\delta\phi] + \frac{\partial\pounds}{\partial\mathbf{u}}[\delta\mathbf{u}] + \frac{\partial\pounds}{\partial\boldsymbol{\lambda}}[\delta\boldsymbol{\lambda}]\,, \tag{33}$$

where $\delta\phi$, $\delta\mathbf{u}$, and $\delta\boldsymbol{\lambda}$ are admissible variations of the respective arguments. For a given ϕ, a point is stationary in relation to $(\mathbf{u},\boldsymbol{\lambda})$ if it satisfies

$$\frac{\partial\pounds}{\partial\boldsymbol{\lambda}}[\delta\boldsymbol{\lambda}] = 0 \quad \text{and} \quad \frac{\partial\pounds}{\partial\mathbf{u}}[\delta\mathbf{u}] = 0\,. \tag{34}$$

Applying condition (34a) in (32), the state equation is recovered. On the other hand, the second condition (34b) provides what is commonly known as adjoint equation:

$$a_\phi(\boldsymbol{\lambda},\delta\mathbf{u}) = -\sum_{r=1}^{Nr}\left\{\left[\alpha_r + c h_r(\mathbf{u},\phi)\right]\frac{\partial h_r(\mathbf{u},\phi)}{\partial\mathbf{u}}[\delta\mathbf{u}]\right\} = 0 \quad \forall\delta\mathbf{u} \in V. \tag{35}$$

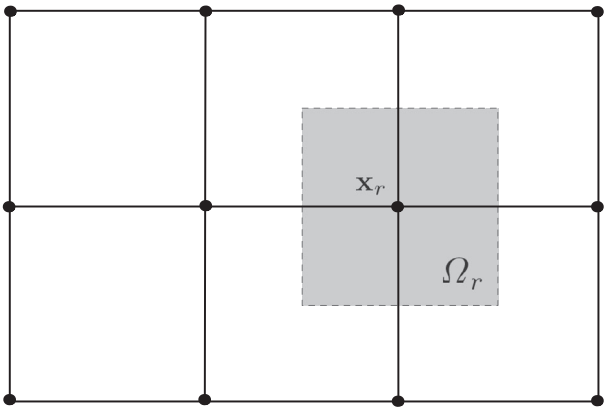

Figure 5. Example of a sample point $\mathbf{x}_r$ (coinciding with a node of the finite element mesh) and its neighborhood Ω_r.

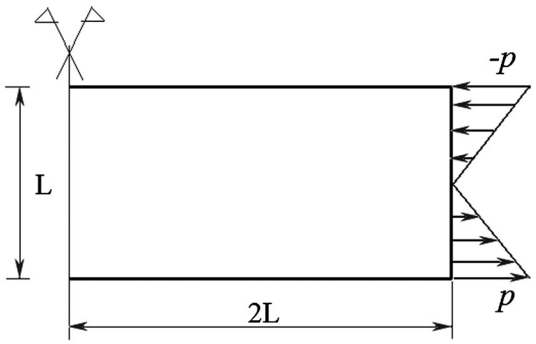

Figure 6. Beam problem.

DOI: 10.1002/nme

It is shown in detail in the Appendix that the derivative of $h_r(\mathbf{u},\phi)$ takes the form

$$\frac{\partial h_r(\mathbf{u},\phi)}{\partial \mathbf{u}}[\delta\mathbf{u}] = \mathbf{C}_r\mathbf{A}_r(\mathbf{u},\phi)\cdot\boldsymbol{\varepsilon}_r(\delta\mathbf{u}), \tag{36}$$

where $\mathbf{A}_r(\mathbf{u},\phi)$, given by Equation (A.11), is a tensor that contains the derivatives of the stress constraints with respect to the stress invariants. Substituting (36) in (35),

$$a_\phi(\boldsymbol{\lambda},\delta\mathbf{u}) = -\sum_{r=1}^{Nr}[\alpha_r + ch_r(\mathbf{u},\phi)]\,\mathbf{C}_r\mathbf{A}_r(\mathbf{u},\phi)\cdot\boldsymbol{\varepsilon}_r(\delta\mathbf{u}) \quad \forall\delta\mathbf{u}\in V, \tag{37}$$

whose solution provides the adjoint field $\boldsymbol{\lambda}$. Finally, the partial derivative of $\pounds(\phi,\mathbf{u},\boldsymbol{\lambda})$ with respect to ϕ is

$$\begin{aligned}\frac{\partial \pounds}{\partial\phi}[\delta\phi] = &\int_D[(\rho_1-\rho_2)+(\mathbf{C}_1-\mathbf{C}_2)\boldsymbol{\varepsilon}(\mathbf{u})\cdot\boldsymbol{\varepsilon}(\boldsymbol{\lambda})]\frac{\partial H(\phi)}{\partial\phi}[\delta\phi]\,dD\\ &+\sum_{r=1}^{Nr}\left\{[\alpha_r+ch_r(\mathbf{u},\phi)]\frac{\partial h_r(\mathbf{u},\phi)}{\partial\phi}[\delta\phi]\right\} \quad \forall\mathbf{u},\boldsymbol{\lambda}\in V.\end{aligned} \tag{38}$$

Because $h_r(\mathbf{u},\phi) = \max\left\{g_r(\mathbf{u},\phi); -\frac{\alpha_r}{c}\right\}$, two cases are possible:

(1) If $h_r(\mathbf{u},\phi) = g_r(\mathbf{u},\phi)$, then

$$\frac{\partial h_r(\mathbf{u},\phi)}{\partial\phi}[\delta\phi] = \frac{\sigma_r^{vM}}{\sigma_{adm}}\frac{\partial\Psi(H_r(\phi))}{\partial H_r(\phi)}\frac{\partial H_r(\phi)}{\partial\phi}[\delta\phi], \tag{39}$$

$$\frac{\partial H_r(\phi)}{\partial\phi}[\delta\phi] = \frac{1}{a_r}\int_D I_r(\mathbf{x})\frac{\partial H(\phi)}{\partial\phi}[\delta\phi]\,dD, \tag{40}$$

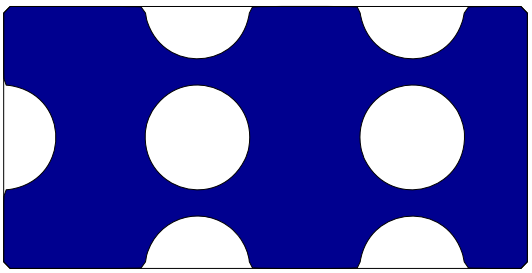

Figure 7. Beam problem: initial level set domain.

Figure 8. Beam problem: optimal structure with mass ratio=0.4628.

DOI: 10.1002/nme

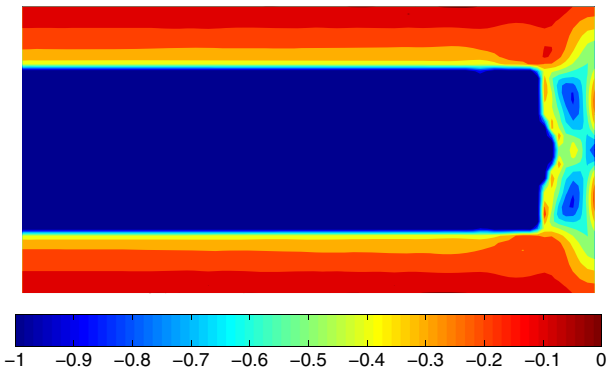

Figure 9. Beam problem: stress constraint distribution ($\max_D(g_r) = 6.2 \times 10^{-3}$).

and thus,

$$\frac{\partial h_r(\mathbf{u},\phi)}{\partial \phi}[\delta\phi] = \int_D \frac{I_r(\mathbf{x})}{a_r}\frac{\sigma_r^{vM}}{\sigma_{adm}}\frac{\partial \Psi(H_r(\phi))}{\partial H_r(\phi)}\frac{\partial H(\phi)}{\partial \phi}[\delta\phi]\, dD. \tag{41}$$

(2) If $h_r(\mathbf{u},\phi) = -\frac{\alpha_r}{c}$, then

$$\frac{\partial h_r(\mathbf{u},\phi)}{\partial \phi}[\delta\phi] = 0. \tag{42}$$

To end this issue, let us call upon the identity[‡]

$$\frac{\partial H(\phi)}{\partial \phi}[\delta\phi] = \delta(\phi)\delta\phi,$$

where $\delta(\phi)$ is the Dirac function. Let us also assume then that the state $(\phi, \mathbf{u}, \boldsymbol{\lambda})$ satifies the equations in (34), that is, state and adjoint equations. Therefore, the variation of the Lagrangian function (32) is given by

$$\delta\pounds(\phi,\mathbf{u},\boldsymbol{\lambda}) = \frac{\partial \pounds}{\partial \phi}[\delta\phi] = \frac{dJ}{d\phi}[\delta\phi] = \int_D G(\phi)\delta(\phi)\delta\phi\, dD, \tag{43}$$

where

$$G(\phi) = \begin{cases} (\rho_1-\rho_2) + (\mathbf{C}_1-\mathbf{C}_2)\boldsymbol{\varepsilon}(\mathbf{u})\cdot\boldsymbol{\varepsilon}(\boldsymbol{\lambda}) \\ \quad + \sum_{r=1}^{Nr}\left\{[\alpha_r + c g_r(\mathbf{u},\phi)]\frac{I_r(\mathbf{x})}{a_r}\frac{\sigma_r^{vM}}{\sigma_{adm}}\frac{\partial\Psi(H_r(\phi))}{\partial H_r(\phi)}\right\}, \quad \text{if } g_r(\mathbf{u},\phi) \geqslant -\frac{\alpha_r}{c}, \\ (\rho_1-\rho_2) + (\mathbf{C}_1-\mathbf{C}_2)\boldsymbol{\varepsilon}(\mathbf{u})\cdot\boldsymbol{\varepsilon}(\boldsymbol{\lambda}), \quad \text{if } g_r(\mathbf{u},\phi) < -\frac{\alpha_r}{c}, \end{cases} \tag{44}$$

it is known as shape gradient density [45, 46].

3.2. *Velocity field*

A Taylor expansion of the objective function is formally given by

$$J(\phi + t\delta\phi) = J(\phi) + t\frac{dJ}{d\phi}[\delta\phi] + \vartheta\left(t^2\right). \tag{45}$$

It is shown in the literature (see, for example, [18, 19]) that choosing $\delta\phi$ based on (31)

[‡]Verify the distinction in notation between the variation $\delta\phi$ and the Dirac function $\delta(\phi)$.

DOI: 10.1002/nme

$$\delta\phi = \frac{\partial\phi}{\partial t} = v_n\|\nabla\phi\|, \tag{46}$$

with

$$v_n = -G(\phi), \tag{47}$$

it is obtained that, for a small enough $t > 0$, the value of J decreases:

$$J(\phi + t\delta\phi) = J(\phi) - t\int_D G^2(\phi)\delta(\phi)\|\nabla\phi\|dD + \vartheta\left(t^2\right) < J(\phi). \tag{48}$$

In other words, using $v_n = -G(\phi)$ in the solution of the level set equation (31) is equivalent to move the boundary $\partial\Omega$ in direction $v_n\mathbf{n}$ with an amplitude proportional to the period of time integration $[0, T]$. The choice of a value for T will be justified later.

3.3. Level set regularization and treatment on the normal velocity field

It is also known that in order to obtain efficient minimization sequences, different improvements on v_n are convenient, so long as they satisfy descent condition (48).

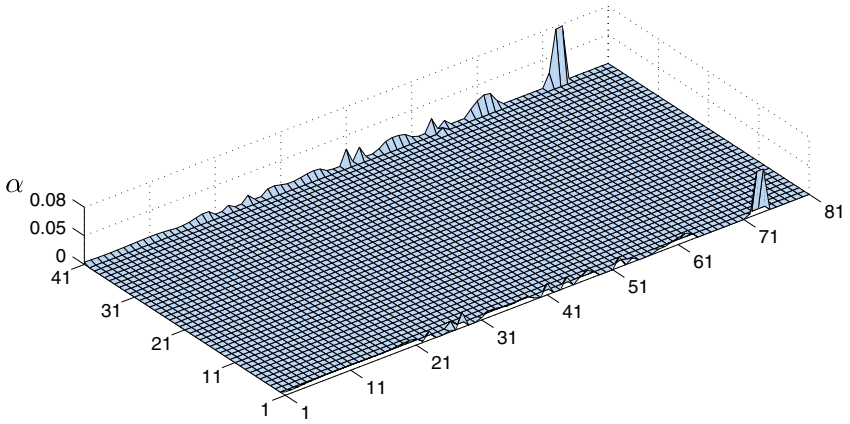

Figure 10. Beam problem: distribution of the Lagrange multipliers at each node in the last iteration.

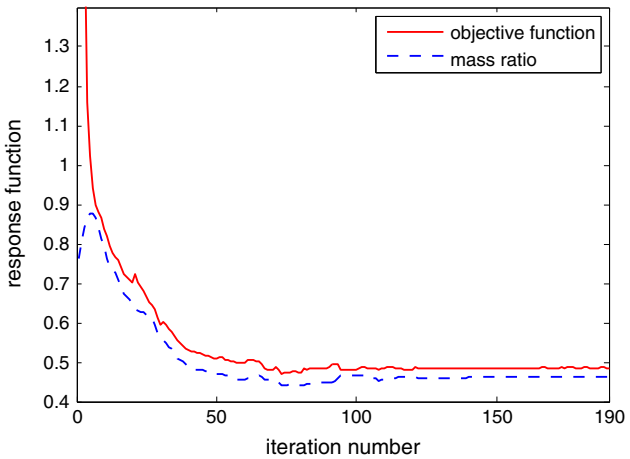

Figure 11. Beam problem: convergence of the objective function and mass ratio.

DOI: 10.1002/nme

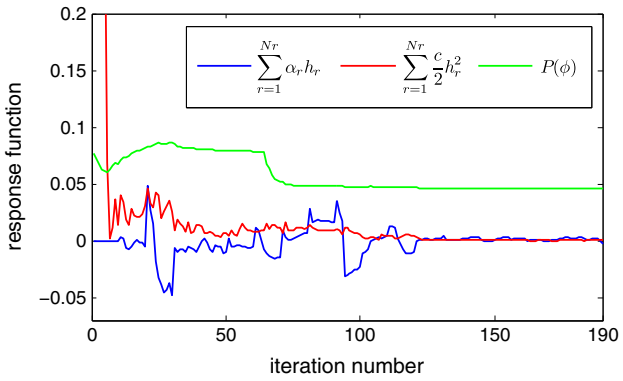

Figure 12. Beam problem: convergence of the penalty terms of the objective function.

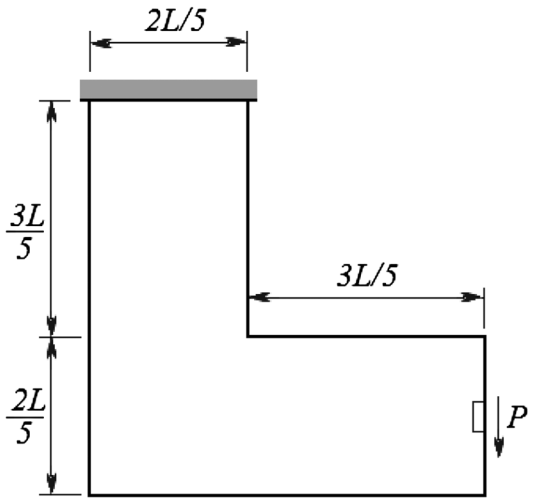

Figure 13. L-problem: model.

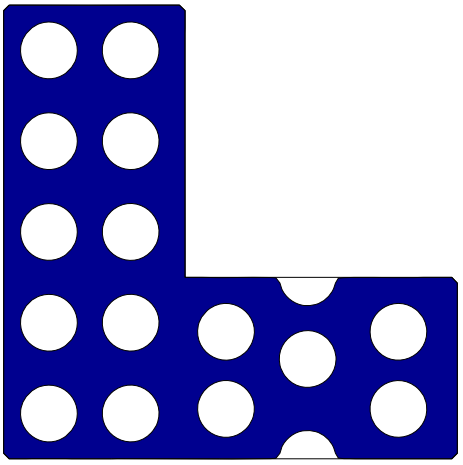

Figure 14. L-problem: initial level set domain for Figures 15–18.

DOI: 10.1002/nme

The first consideration is related to the inclusion of a classic perimeter regularization that has the effect of smoothening the boundary [46, 47]. A consistent way of doing that is by modifying the objective function by the addition of a perimeter penalization term $P(\phi)$:

$$\bar{J}(\phi) := J(\phi) + P(\phi), \tag{49}$$

$$P(\phi) = \int_D \mu \delta(\phi) \|\nabla \phi\| dD, \tag{50}$$

where $\mu > 0$ is a penalization factor. Deriving this new expression, it is easy to show that the field $G(\phi)$ modifies to

$$\bar{G}(\phi) := G(\phi) - \mu\kappa \ , \quad \kappa = \operatorname{div} \mathbf{n}, \tag{51}$$

where κ plays the role of average curvature of the level set.

Other observed phenomenon in the present problem is that the velocity field (44) has severe variations in amplitude as a consequence of local stress constraints naturally appearing because of arbitrary moving geometries. This characteristic has the undesirable effect of locking the boundary: only very limited portions of the boundary moves, while all the rest remains almost static. To avoid this effect, we propose a modified definition for v_n that provided significant improvements:

$$G_{\log}(\phi) = \begin{cases} \ln(\bar{G}(\phi) + 1), & \text{if } \bar{G}(\phi) \geqslant 0, \\ -\ln(-\bar{G}(\phi) + 1), & \text{if } \bar{G}(\phi) < 0. \end{cases} \tag{52}$$

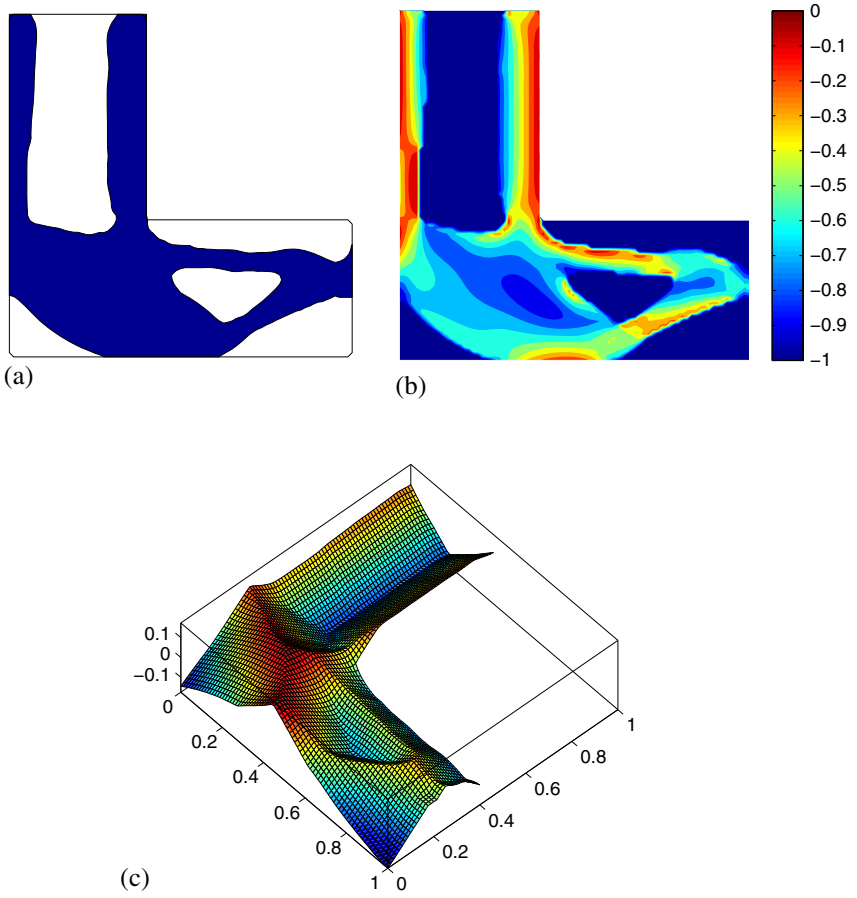

Figure 15. L-problem: (a) optimal structure; (b) stress constraint distribution for $q = 0.25$; and (c) level set surface of the optimal structure. The mass ratio is 0.5437 and $\max_D(g_r) = 3.5 \times 10^{-3}$.

DOI: 10.1002/nme

Because this operation preserves the signal of v_n, it also satisfies the descent condition (48).

In addition, although the field $G_{\log}(\phi)$ calculated in (52) is defined everywhere, just its value on the boundary $\partial\Omega$ should be accounted for in (48). Among different techniques available to extend/regularize this field over D [17, 19, 47], the most performing for the present case was the Hilbertian method proposed in [48], providing a new velocity field $G^*(\phi)$ from $G_{\log}(\phi)$. Finally, after performing all operations earlier, the velocity field v_n is normalized by

$$v_n = \frac{-G^*(\phi)}{\max(|G^*(\phi)|)}. \tag{53}$$

4. DISCRETIZATION AND NUMERICAL IMPLEMENTATION

The finite element method (FEM) is employed to solve the state equation (10) and the adjoint equation (37). The problem is generically formulated for any dimension but tested here with only 2D numerical examples under plane stress conditions. For the implementation of the examples, we used a single mesh to discretize the level set function and for the analysis of finite elements, which uses a quadrilateral bilinear element.

For the discrete solution of the Hamilton–Jacobi equation (31), an upwind finite difference scheme is used. Furthermore, a reinitialization procedure is performed to maintain the level set function as a signed distance function. For details about the numerical solution schemes for Equation (31), we refer the readers to [18, 19, 27, 28].

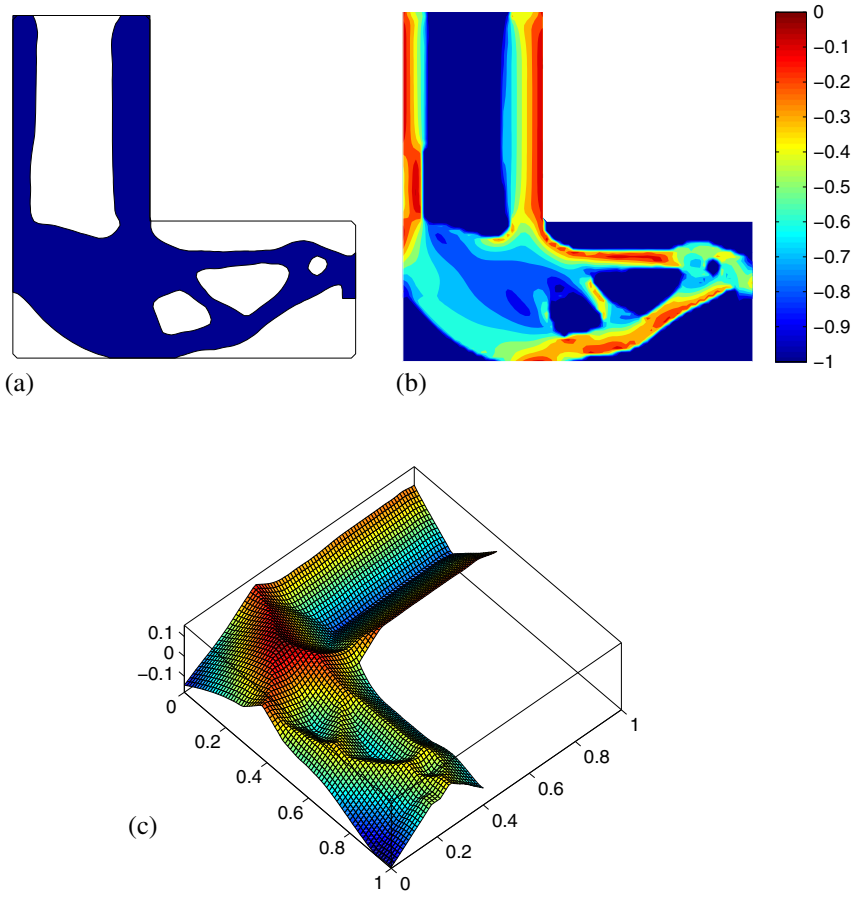

Figure 16. L-problem: (a) optimal structure; (b) stress constraint distribution for $q = 0.5$; and (c) level set surface of the optimal structure. The mass ratio is 0.5099 and $\max_D(g_r) = 2.3 \times 10^{-3}$.

DOI: 10.1002/nme

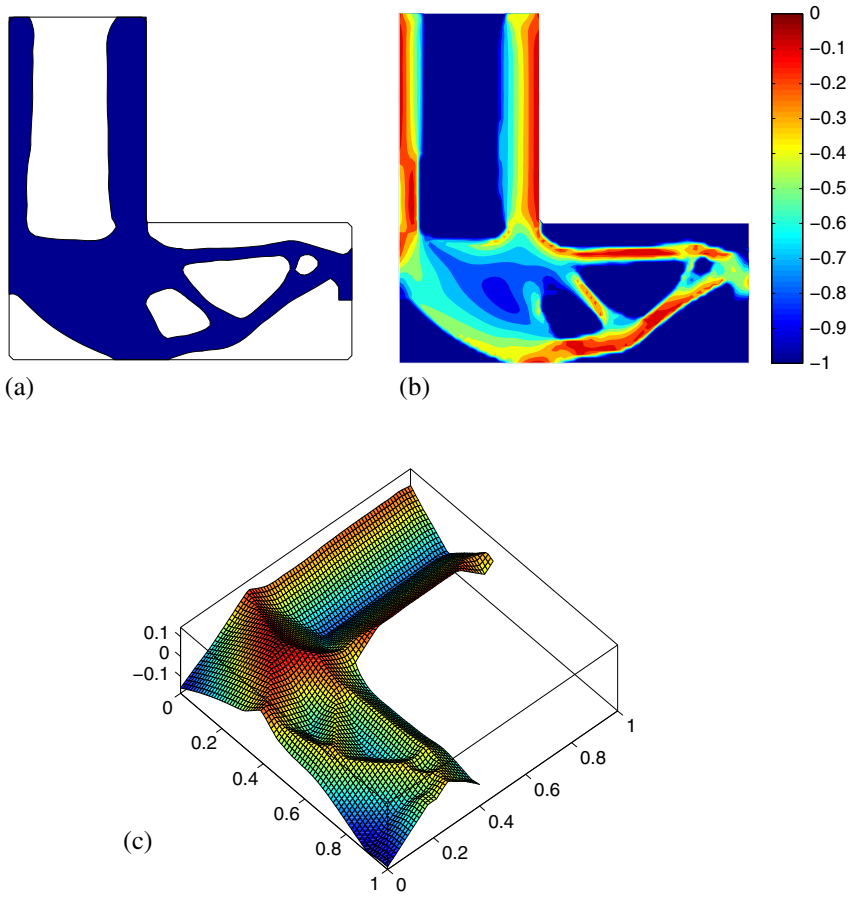

Figure 17. L-problem: (a) optimal structure; (b) stress constraint distribution for $q = 0.75$; and (c) level set surface of the optimal structure. The mass ratio is 0.4802 and $\max_D(g_r) = 5.1 \times 10^{-3}$.

4.1. Optimization algorithm

With the sensitivity analysis of (44), we naturally defined a velocity field v_n for the level set equation (31). The optimization process should lead the structure to a local optimal design. The optimization algorithm to solve Problem P_4 is then summarized in the succeeding text:

External loop:

(1) Initialization of the level set function ϕ^0 as a signed distance function defining the initial guess $\Omega_0 \subset D$.
(2) Define $k = 1$, $c^k > 0$, $\alpha_r^k \in \mathbb{R}$.
(3) Perform the *internal loop* to minimize function $J^k\left(\phi, \alpha_r^k, c^k\right)$ obtaining ϕ^k.
(4) Update c^k and α_r^k using (29).
(5) $k = k + 1$. Return to step 3.

The step 3 of the *external loop*, called *internal loop*, consists of the minimization of objective function J^k for fixed given values of c^k and α_r^k. However, as indicated in [44], the minimization in 3 may be performed partially or, equivalently, substituted by a sufficient descent condition. For practical purposes, this means that a fixed number of minimization iterations, say $Niter$, must be accomplished prior to the Lagrange multipliers updating in 4. Then, the iterative procedure for a sufficient decrease of $J^k(\phi, \alpha_r^k, c^k)$ is the following:

DOI: 10.1002/nme

Internal loop: for $j = 1$ *to* $j \leqslant Niter$:

(1) Obtain the discretized fields $\mathbf{u}_j$ and $\boldsymbol{\lambda}_j$ by solving, respectively, the state equation (26) and adjoint equation (37).
(2) Compute the velocity field $v_{nj}(\mathbf{u}_j, \boldsymbol{\lambda}_j)$ by means of Equation (53).
(3) Solve the level set equation during a time integration period ΔT_j, $T_{j+1} = T_j + \Delta T_j$, chosen such that $J(\phi_{j+1}) \leqslant J(\phi_j)$.
(4) If $\left|J(\phi_{j+1}) - J(\phi_j)\right| \leqslant \varepsilon$, then stop the iterative process; otherwise continue.
(5) $j = j + 1$. Go to step 1.

The discrete version of the level set equation (31) is given by

$$\phi^{i+1} = \phi^i - \Delta t \left(v_{nj} \|\nabla \phi^i\|\right), \tag{54}$$

where $i = 1 \ldots m$ is the number of level set updatings for a given normal velocity v_{nj} during the time integration period $\Delta T_j = m\Delta t$. The time integration period ΔT_j is analogous to the step size of a line search minimization in the descent direction provided by the velocity v_{nj}. The number of updatings m is conveniently chosen to satisfy a descent condition given in step 3 of the internal minimization loop. The numerical technique used here is an explicit first-order upwind scheme (see, for example, [27, 28]) where Δt must satisfy the so-called CFL condition:

$$\Delta t = \Delta t_{CFL} \leqslant \frac{\min(\Delta x)}{\max |v_n|}, \tag{55}$$

being Δx the minimum grid size.

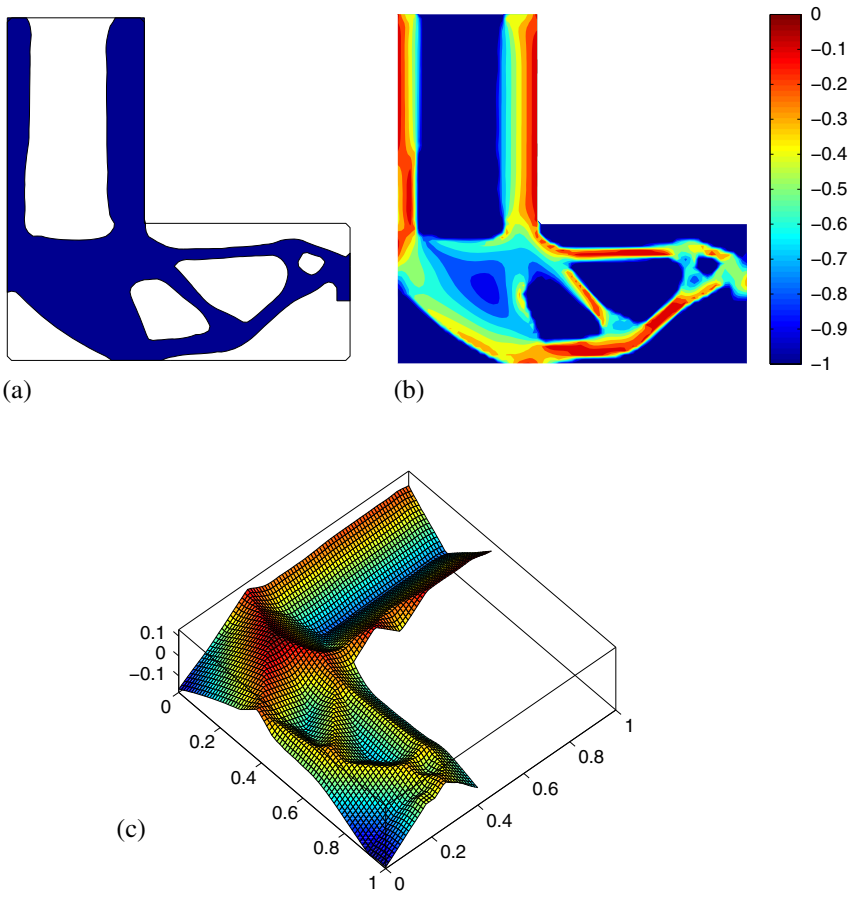

Figure 18. L-problem: (a) optimal structure; (b) stress constraint distribution for $q = 1$; and (c) level set surface of the optimal structure. The mass ratio is 0.4598 and $\max_D(g_r) = 2.1 \times 10^{-3}$.

DOI: 10.1002/nme

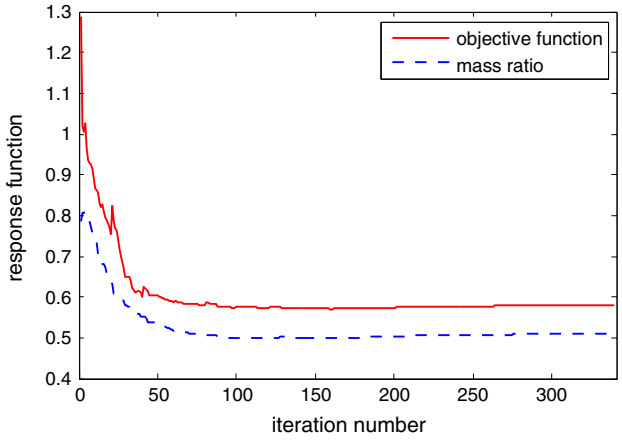

Figure 19. L-problem: convergence of the objective function and mass ratio for $q = 0.5$.

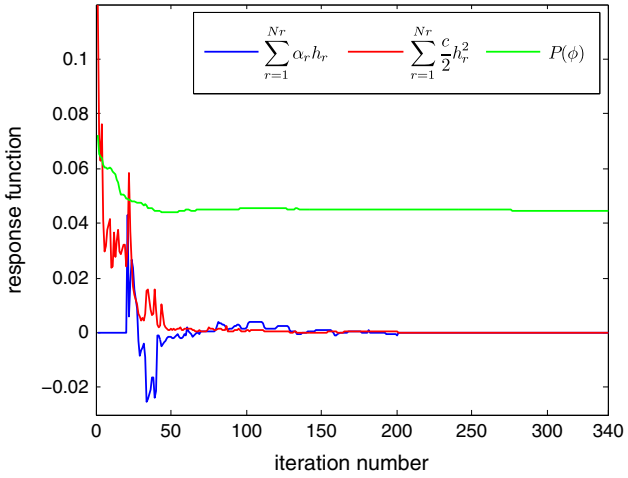

Figure 20. L-problem: convergence of the penalty terms of the objective function for $q = 0.5$.

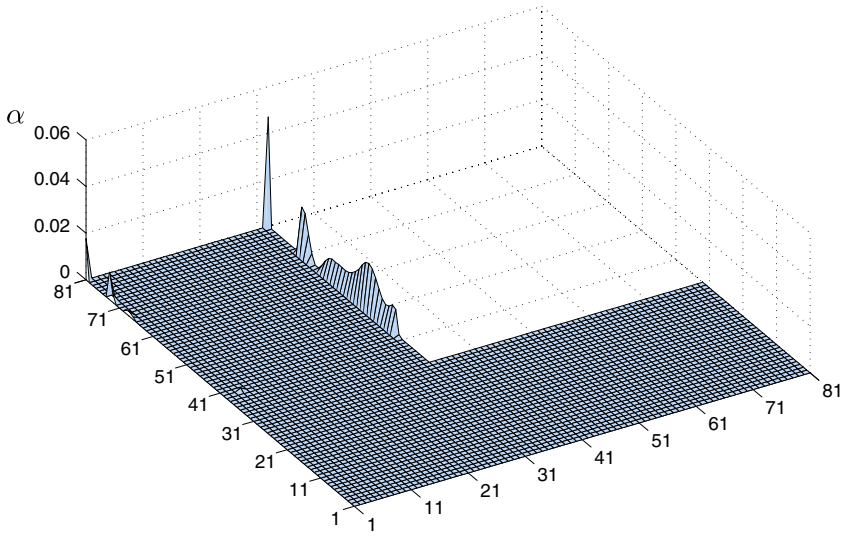

Figure 21. L-problem: distribution of the Lagrange multipliers at each node in the last iteration for the case where $q = 0.5$.

DOI: 10.1002/nme

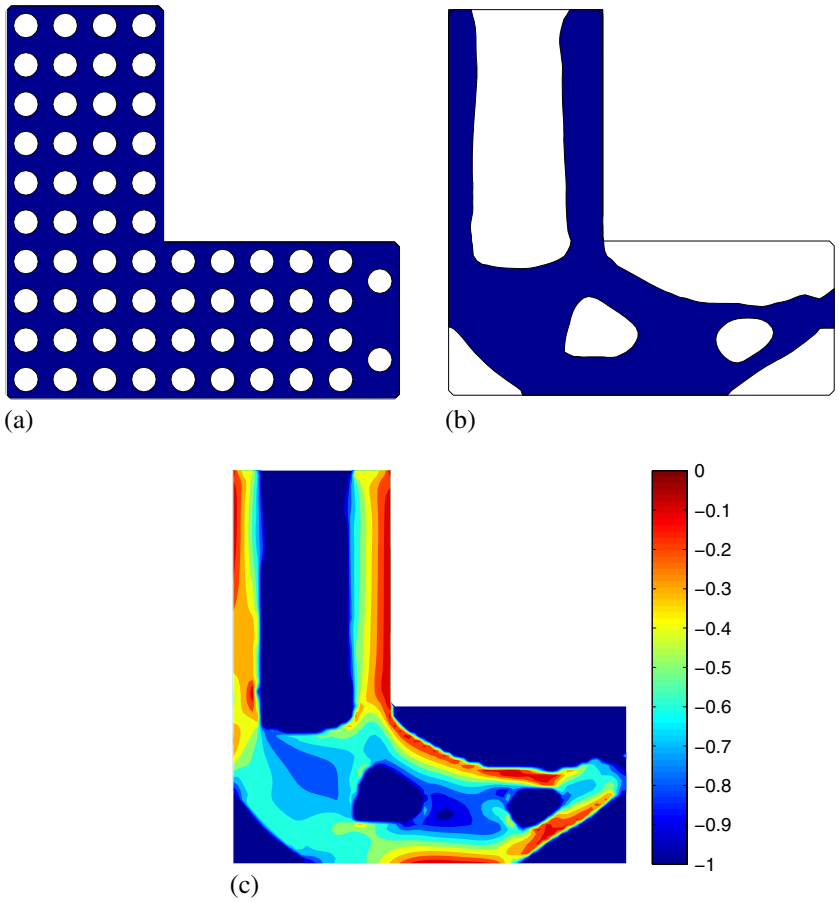

Figure 22. L-problem: (a) initial level set domain; (b) obtained design for $q = 0.5$; and (c) stress constraint distribution with $\max_D(g_r) = 5.6 \times 10^{-3}$. The mass ratio is 0.5066.

It has been noted in the numerical experiments that parameters m (associated to the time integration period) and $Niter$ (associated to the number of internal loops) have appreciable influence on the final optimal configuration. The first one is somehow limited by the descent condition of step 3 of the internal loop. In the present implementation, the objective function is tested periodically, and the time integration period ΔT_j is chosen when $J(\phi_j)$ stops decreasing (similarly to an inexact step determination). The choice of $Niter$ is more heuristical. At present, it has been chosen $Niter = 20$ in most cases, unless particular cases indicated.

4.2. Sample points stress evaluation

In the present implementation, the sample points $\mathbf{x}_r$ do coincide with the nodes of the finite element mesh. This distribution of sample points is consistent with the objective of enforcing the stress constraint all over the domain. It is then possible to say that with this choice, the number and position of sample points follow the resolution of the stress field provided by the finite element mesh. The corresponding neighborhood Ω_r is squared with a length of a finite element size (Figure 5). In this way, there is no overlapping among distinct neighborhoods, that is, $\Omega_{r_i} \cap \Omega_{r_j} = \emptyset$ for $i \neq j$, and all of domain D is covered by the neighborhoods.

Moreover, because bilinear quadrilateral elements are used, the strain field is discontinuous among elements. Thus, the strain $\boldsymbol{\varepsilon}_r(\mathbf{x}_r)$ at a node $\mathbf{x}_r$ is computed using a classical recovering technique given by the average of the elementar strains attached to the node:

DOI: 10.1002/nme

$$\boldsymbol{\varepsilon}_r(\mathbf{U}) = \sum_{e=1}^{N_e} \frac{\mathbf{B}_e(\mathbf{x}_r)\mathbf{U}_e}{N_e}, \tag{56}$$

where N_e is the number of elements e attached to node $\mathbf{x}_r$, $\mathbf{B}_e(\mathbf{x}_r)$ is the array of shape function derivatives of element e, and $\mathbf{U}_e$ is the array of nodal displacements of element e. The stress at this node is then computed by (18) and the stress constraint by (22) where the value of $H_r(\phi)$ was computed using the procedure proposed in [49] in which an exact Heaviside function is used.

5. NUMERICAL RESULTS

In all examples, the densities of the solid and weak materials are respectively $\rho_1 = 1$ and $\rho_2 = 10^{-3}$. The Young's modulus of the solid material is normalized to $E = 1$ and $E_2 = 10^{-3}$ Pa for the weak material. The Poisson's ratio is set at $\nu = 0.3$. In the loading region, it is assumed that the boundary Γ_N is kept fixed during the whole optimization process, that is, $\phi(\Gamma_N, t) \equiv 0\ \forall t$. Besides this, it is imposed that velocity v_n at the boundary Γ_N is null. The examples are presented in 2D under plane stress state.

The number of sample points where the stress constraint is evaluated coincide with the number of nodes in the mesh. The Lagrange multiplier vectors are initialized with a vector of zeroes, and the maximum penalization factor is limited as $c_{\max} = 10c$.

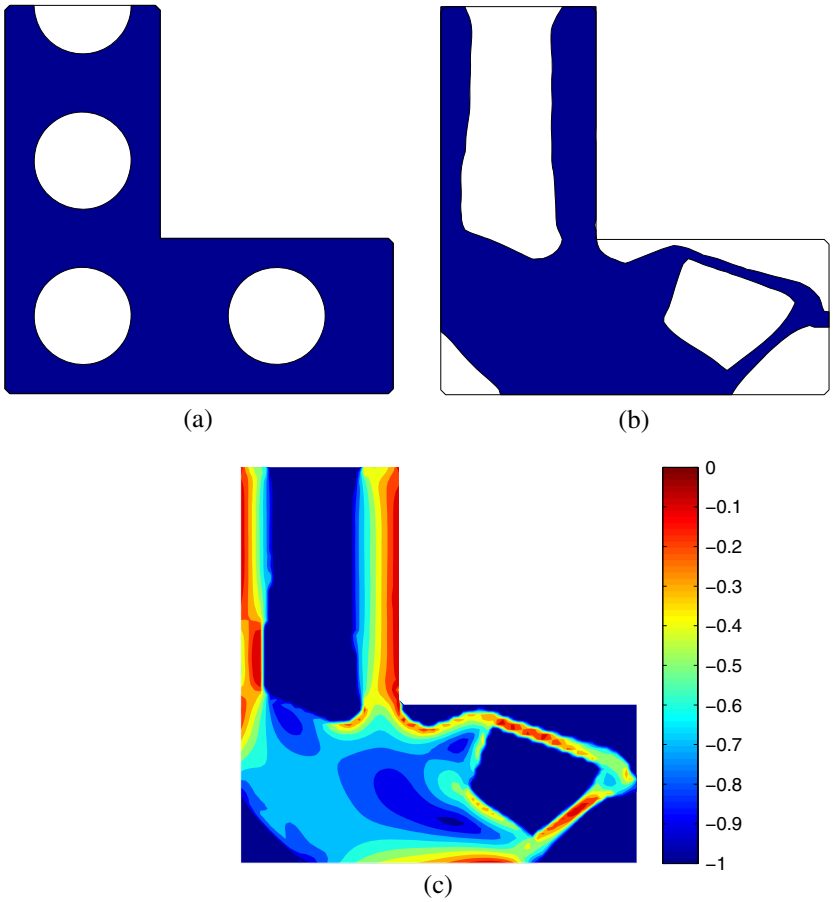

Figure 23. L-problem: (a) initial level set domain; (b) obtained design for $q = 0.5$; and (c) stress constraint distribution with $\max_D(g_r) = 1.7 \times 10^{-3}$. The mass ratio is 0.5630.

DOI: 10.1002/nme

At each iteration j of the *internal loop*, a number $m \leqslant 32$ of the first-order scheme (54) updatings are performed with a time step Δt set up to $\Delta t = 0.1(\min(\Delta x)/\max|v_n|)$. The number m may be less than 32, once the descent condition 3 of the internal loop is satisfied. The value of Δt may also be reduced if the objective function is not decreasing.

Concerning reinitialization, the classical scheme given in [27, 28] to recover a signed distance function was used. In the examples in the succeeding text, the level set function was reinitialized every four updating steps.

The extension/regularization treatment for v_n described in Section 3.3 was used in all numerical examples. In all converging diagrams, each iteration corresponds to a normal velocity v_{nj} calculation, that is, to an iteration of the *internal loop.*

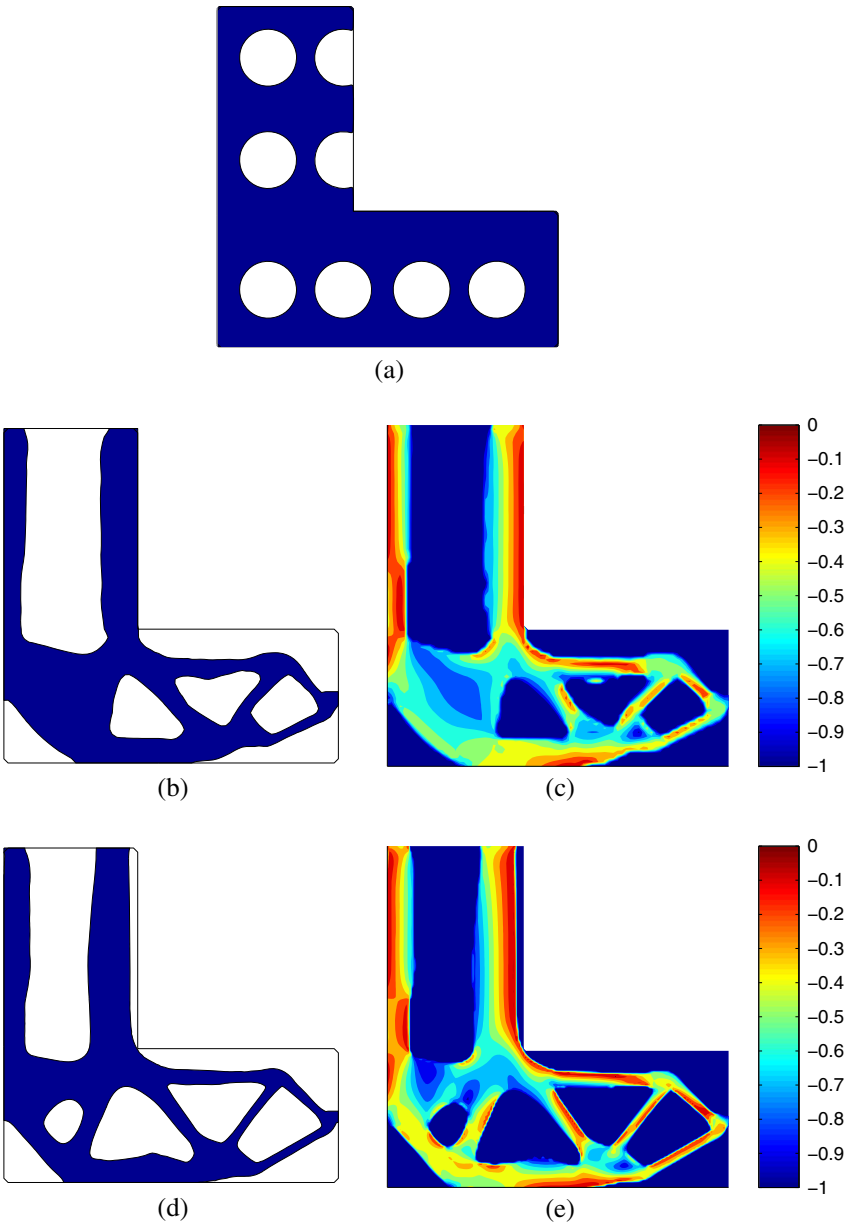

Figure 24. L-problem: results for different meshes and $q = 0.5$; (a) initial level set domain; (b) final design for coarse mesh (mass ratio = 0.4791); (c) stress constraints distribution for coarse mesh ($\max_D(g_r) = 3.2 \times 10^{-3}$); (d) final design for refined mesh (mass ratio=0.4623); and (e) stress constraints distribution for refined mesh ($\max_D(g_r) = 4.0 \times 10^{-3}$).

DOI: 10.1002/nme

5.1. Beam problem

The first example deals with a pure bending of a beam. Domain D is the rectangle shown in Figure 6 with $L = 1$ m. A pure moment is applied with a convenient pressure distribution with maximum value of $p = 30$ Pa varying linearly from the axis of the beam. The yield stress is $\sigma_{adm} = 35$ Pa. Considering symmetry, a mesh of 80×40 is used for half the structure. The initial level set is shown in Figure 7.

The following parameters were used: $q = 0.5$ for the exponent in (23), penalization factor $c = 0.08$, updating $\beta = 1.2$ and $\mu = 0.01$ for the perimeter regularization. The optimization procedure was stopped after 19 external iterations considering a number of iterations $Niter = 10$ for the internal optimization loop.

The final result is displayed in Figure 8 where an I-like profile was achieved, similar to that obtained in [2]. The mass ratio (final mass/total mass) is 0.4628 in the optimal structure. In Figure 9 is shown the distribution of (nodal) stress constraints. As expected, in the inner part of the horizontal bars, the stress constraint function is inactive, being close to zero on the external regions. The maximum value achieved for the constraints is $\max_D(g_r) = 6.2 \times 10^{-3}$, which means a small violation.

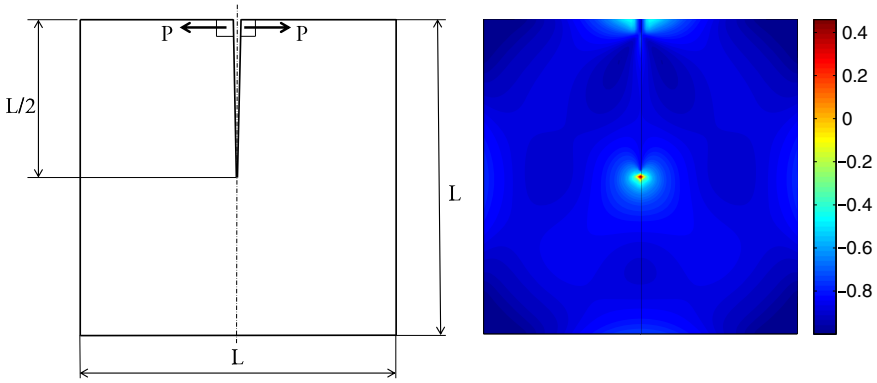

Figure 25. Crack problem: model and stress constraint distribution with high stress concentration at the fracture tip ($\max_D(g_r) = 0.4628$).

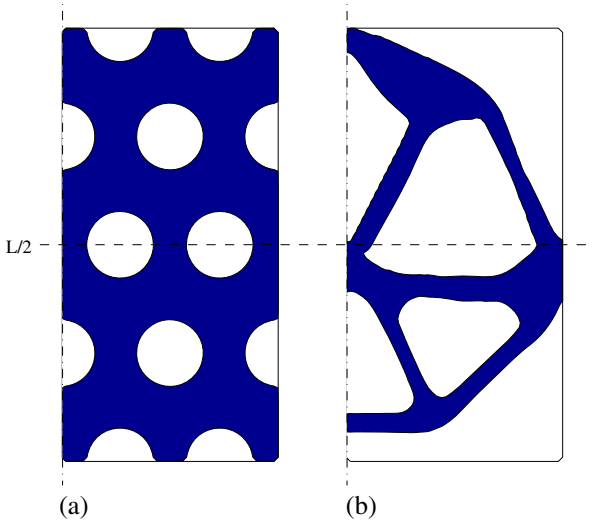

Figure 26. Crack problem: (a) initial level set domain and (b) optimal structure for $q = 0.5$. The mass ratio is 0.2945.

DOI: 10.1002/nme

This correlates to the distribution of the Lagrange multiplier values at the nodes shown in Figure 10. Note that most of them have zero value except those nodes of constraint activation. In addition, the distribution is quite regular, suggesting a good behavior of the algorithm. The history of the objective function is seen in Figure 11. Figure 12 shows the linear and quadratic contributions of the stress penalization terms (Equation (25)) converging to zero as expected and the convergence history of the perimeter constraint $P(\phi)$.

5.2. *L-problem*

This example is the classic benchmark problem of topology optimization considering stress constraints. Figure 13 shows the model clamped at its top boundary and submitted to a resultant force $P = 1$ N applied at the middle of the right side. The length is $L = 1$ m, and the yield stress $\sigma_{adm} = 42$ Pa.

Domain D was discretized with 80 elements along the longest sides in both horizontal and vertical directions giving a total of 4,096 quadrilateral finite elements and 4,257 nodes. Therefore, there exist $N_r = 4,257$ sample points for the stress evaluation. The optimization was run using the following parameters: $c = 0.15$, $\beta = 1.2$, and $\mu = 0.01$. The exponent q was tested for the following

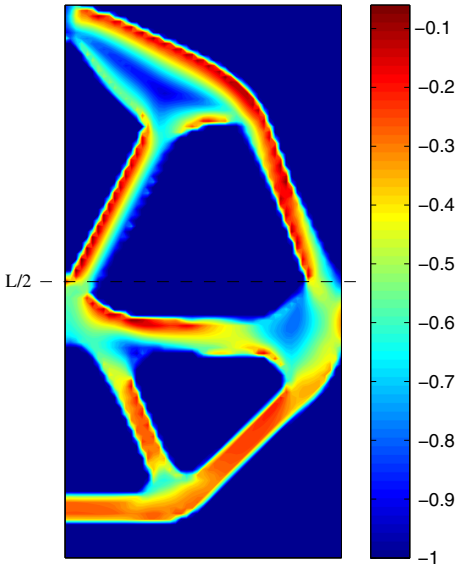

Figure 27. Crack problem: stress constraint distribution for $q = 0.5$ ($\max_D(g_r) = -5.04 \times 10^{-2}$).

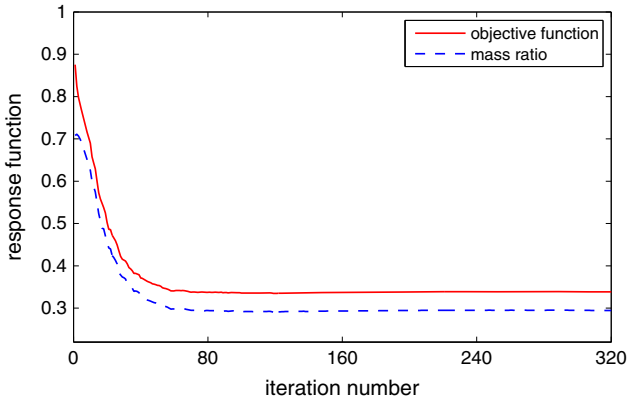

Figure 28. Convergence of the objective function and mass ratio for the crack problem ($q = 0.5$).

DOI: 10.1002/nme

values: $q = 0.25$, $q = 0.5$, $q = 0.75$, and $q = 1$. From the initial level set domain in Figure 14, the corresponding final designs and the constraint distribution for each of the four cases are shown in Figure 15–18. From the final mass ratio of each case, it is possible to see that the smaller the value of q, the more robust the design. This is consistent with the proposed constraint expression in which the stress of points localized near the boundary (even outside of it) are progressively considered as q decreases. It must be observed that in all cases *including the case* $q = 1$, *that is, no enhancement*, the reentrant corner with high stress concentration is eliminated with a well-defined arch. It is important to emphasize that among the four cases run the maximum value of the stress constraint is $\max_D(g_r) = 5.1 \times 10^{-3}$.

The convergence history of the objective function for $q = 0.5$ is shown in Figure 19. In this case, the minimization was stopped after 17 updates of external loop and $Niter = 20$ fixed iterations for each subproblem (internal loop). Figure 20 shows the convergence of the penalty terms of the objective function (both figures for $q = 0.5$). The distribution of the Lagrange multipliers is shown in Figure 21.

A characteristic of the level set method is the dependence of the final design in relation to the initialization. Figures 22 and 23 show different initializations. To improve convergence, the penalization factor values were modified to $c = 0.1$ and $c = 0.18$, respectively. We used $q = 0.5$ for both examples. The optimal structures obtained at the end of the optimization process satisfy the constraints imposed in the problem. The layouts are quite different from the previously obtained; however, the rounding radius of the corner shows that the stress concentration has been detected and eliminated.

Finally, two mesh sizes were compared. The first one is that used in the previous cases, while the second has 160 elements along the longest sides in both horizontal and vertical directions, totaling 16,384 quadrilateral finite elements and 16,705 nodes. Figure 24 shows the results obtained.

5.3. *Crack problem*

This example emulates the fracture mode I of a squared plate of length $L = 1$ m and fracture length $L/2$. A unitary force is applied to open the fracture therefore producing high stresses at the fracture tip (Figure 25). The main objective of this example is to verify if the proposed approach is able to achieve a feasible design and a local minimum for the mass. Only the right symmetric part of the plate was partitioned with a mesh of 100×50 elements and 5,151 nodes (equal to the number of stress sample points). The following parameters were used: $q = 0.5$, $c = 0.3$, $\beta = 1.2$, and $\mu = 0.01$. The yield stress is $\sigma_{adm} = 23$ Pa. The initial and final configurations are shown in Figure 26(a) and (b), respectively. The final design eliminates the stress singularity, and a feasible design is achieved. The distribution of the stress constraint values is shown in Figure 27. The convergence graphs of mass and penalization terms are shown in Figures 28 and 29. It is possible to see that the penalization terms converge to zero, as expected for a feasible design.

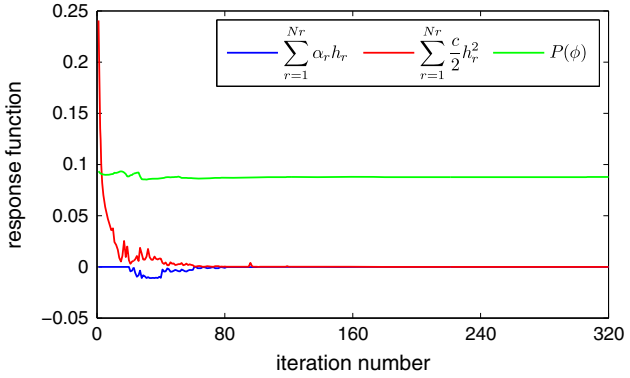

Figure 29. Convergence of the penalty terms of the objective function for the crack problem ($q = 0.5$).

DOI: 10.1002/nme

6. CONCLUDING REMARKS

A new approach combining a level set moving boundary and augmented Lagrangian technique was used to solve the structural (topological) optimization problem of mass minimization under local stress constraints. Some observations should be emphasized:

(1) It is proposed the definition of a neighborhood around each sample point (node) in such a way that the activation of the stress constraint associated to the sample point is proportional to the overlapping between the current domain and the considered neighborhood. In this way, the activation/deactivation of stress constraints associated to the sample points is performed in a continuous way as long as the boundary moves over the background domain D. The stress measured, however, remains *local* in the sense that it represents the stress at $\mathbf{x}_r$ and not its average over a neighborhood.
(2) A stress constraint function was proposed in such a way that enhances the area fraction $H_r(\phi) < 1$ that measures the intersection between Ω and the neighborhood of $\mathbf{x}_r$. This is performed by an exponent $q < 1$. Different values of q were tested with the L-shaped benchmark problem with successful results. Values of $q < 0.25$ reached convergence difficulties due to the almost discontinuous behavior of the stress constraints with respect to the boundary movement. However, it was observed that even in the case with no enhancement, that is, $q = 1$, the stress concentrations are identified and eliminated by rounded boundaries.
(3) A very simple recovering technique was employed to obtain a continuous strain field based on the same bilinear shape functions used for the displacement solution (other techniques could be tested). Then as pointed out in Section 4.2, a distribution of sample points that are coincident with the nodes of the (Lagrangian) mesh is consistent with the objective of enforcing the stress constraint all over the domain. It is then possible to say that with this choice, the number and position of sample points follow the resolution of the stress field provided by the finite element mesh.
(4) The conventional numerical solution of the Hamilton–Jacobi equation based on upwind schemes was used to move the boundary $\partial\Omega$ despite its well-known problems associated to the impossibility of creating new holes and the need of reinitialization [18, 19]. Reinitialization is particularly inconvenient at the end of the minimization process. At this stage, the boundary movements are usually smaller than those undesirably caused by the reinitialization technique, the fact that pollutes the solution and hinders complete convergence.
(5) The velocity field v_n obtained from the sensitivity analysis showed to be a proper descent direction. However, the regularization techniques proposed in Section 3.3 were crucial to avoid premature locking of the boundary movement. The velocity field seems to show a quite irregular distribution due to the characteristics of the adjoint solution. High stiffness rations between material phases 1 and 2 as well as stress constraints cause peak values in the adjoint solution that are transferred to v_n. This difficulty has been overcome here using the proposed logarithmic scaling (expression (52)) and the Hilbertian velocity extension proposed by [48] to regularize the distribution of v_n along D.
(6) The classical benchmark example L-shape was tested for several initial level sets, driving to different final solutions. The important challenge of feasibility was successfully overcome in all cases. The optimization algorithm identified the stress concentration and drove to designs that eliminated undesired corners.

APPENDIX: DERIVATIVE OF THE FAILURE FUNCTION

A material failure criterion consists of a function g capable of identifying how far a material point submitted to a quasi-static stress state is from failure. It is a usual approach to write the failure function of any isotropic material as

$$g(I_1, J_2, J_3, k_1, k_2, \ldots) = 0, \tag{A.1}$$

DOI: 10.1002/nme

where k_1 and k_2 are material parameters, and I_1, J_2 and J_3 are the three invariants of the stress tensor $\boldsymbol{\sigma}(\mathbf{u})$ given by

$$I_1 = tr[\boldsymbol{\sigma}(\mathbf{u})] = \mathbf{I} \cdot \boldsymbol{\sigma}(\mathbf{u}), \tag{A.2}$$

$$J_2 = \frac{1}{2}\mathbf{s}(\mathbf{u}) \cdot \mathbf{s}(\mathbf{u}), \tag{A.3}$$

$$J_3 = \frac{1}{3}\mathbf{s}(\mathbf{u})\mathbf{s}(\mathbf{u}) \cdot \mathbf{s}(\mathbf{u}), \tag{A.4}$$

where

$$\mathbf{s}(\mathbf{u}) = \mathbf{P}\boldsymbol{\sigma}(\mathbf{u}), \quad \mathbf{P} = \mathbf{II} - \frac{1}{3}\mathbf{I} \otimes \mathbf{I} \tag{A.5}$$

is the tensor of deviatoric stresses.

The derivative of $h_r(\mathbf{u}, \phi)$ in the direction $\delta\mathbf{u}$ may be written as function of the invariants of the stress tensor $\boldsymbol{\sigma}_r$ through the chain rule:

$$\begin{aligned} \frac{\partial h_r(\mathbf{u}, \phi)}{\partial \mathbf{u}}[\delta\mathbf{u}] = & \frac{\partial h_r(\mathbf{u}, \phi)}{\partial I_1}\frac{\partial I_1}{\partial \mathbf{u}}[\delta\mathbf{u}] + \frac{\partial h_r(\mathbf{u}, \phi)}{\partial J_2}\frac{\partial J_2}{\partial \mathbf{u}}[\delta\mathbf{u}] \\ & + \frac{\partial h_r(\mathbf{u}, \phi)}{\partial J_3}\frac{\partial J_3}{\partial \mathbf{u}}[\delta\mathbf{u}]. \end{aligned} \tag{A.6}$$

Calculating the derivatives of the stress invariants in relation to $\mathbf{u}$,

$$\begin{aligned} \frac{\partial I_1}{\partial \mathbf{u}}[\delta\mathbf{u}] = & \left.\frac{\partial}{\partial t}[\mathbf{I} \cdot \boldsymbol{\sigma}_r(\mathbf{u} + t\delta\mathbf{u})]\right|_{t=0}, \\ & = \mathbf{I} \cdot \boldsymbol{\sigma}_r(\delta\mathbf{u}) = \mathbf{I} \cdot \mathbf{C}_r\boldsymbol{\varepsilon}_r(\delta\mathbf{u}), \\ & = \mathbf{C}_r\mathbf{I} \cdot \boldsymbol{\varepsilon}_r(\delta\mathbf{u}), \end{aligned} \tag{A.7}$$

$$\begin{aligned} \frac{\partial J_2}{\partial \mathbf{u}}[\delta\mathbf{u}] = & \left.\frac{\partial}{\partial t}\left[\frac{1}{2}\mathbf{s}_r(\mathbf{u} + t\delta\mathbf{u}) \cdot \mathbf{s}_r(\mathbf{u} + t\delta\mathbf{u})\right]\right|_{t=0}, \\ & = \mathbf{s}_r(\mathbf{u}) \cdot \mathbf{P}\boldsymbol{\sigma}_r(\delta\mathbf{u}), \\ & = \mathbf{P}^T\mathbf{s}_r(\mathbf{u}) \cdot \mathbf{C}_r\boldsymbol{\varepsilon}_r(\delta\mathbf{u}), \\ & = \mathbf{C}_r\mathbf{P}^T\mathbf{s}_r(\mathbf{u}) \cdot \boldsymbol{\varepsilon}_r(\delta\mathbf{u}), \end{aligned} \tag{A.8}$$

$$\begin{aligned} \frac{\partial J_3}{\partial \mathbf{u}}[\delta\mathbf{u}] = & \left.\frac{\partial}{\partial t}\left[\frac{1}{3}\mathbf{s}_r(\mathbf{u} + t\delta\mathbf{u})\mathbf{s}_r(\mathbf{u} + t\delta\mathbf{u}) \cdot \mathbf{s}_r(\mathbf{u} + t\delta\mathbf{u})\right]\right|_{t=0}, \\ & = \mathbf{s}_r(\mathbf{u})\mathbf{s}_r(\mathbf{u}) \cdot \mathbf{P}\mathbf{C}_r\boldsymbol{\varepsilon}_r(\delta\mathbf{u}), \\ & = \mathbf{C}_r\mathbf{P}^T\mathbf{s}_r(\mathbf{u})\mathbf{s}_r(\mathbf{u}) \cdot \boldsymbol{\varepsilon}_r(\delta\mathbf{u}). \end{aligned} \tag{A.9}$$

Here, $\mathbf{s}_r(\mathbf{u})$ is the deviatoric stress tensor of sample point r. Substituting Equation (A.7)-(A.9) in (A.6), we have

$$\frac{\partial h_r(\mathbf{u}, \phi)}{\partial \mathbf{u}}[\delta\mathbf{u}] = \mathbf{C}_r\mathbf{A}_r(\mathbf{u}, \phi) \cdot \boldsymbol{\varepsilon}_r(\delta\mathbf{u}), \tag{A.10}$$

where

$$\mathbf{A}_r(\mathbf{u}, \phi) = \frac{\partial h_r(\mathbf{u}, \phi)}{\partial I_1}\mathbf{I} + \frac{\partial h_r(\mathbf{u}, \phi)}{\partial J_2}\mathbf{P}^T\mathbf{s}_r(\mathbf{u}) + \frac{\partial h_r(\mathbf{u}, \phi)}{\partial J_3}\mathbf{P}^T\mathbf{s}_r(\mathbf{u})\mathbf{s}_r(\mathbf{u}), \tag{A.11}$$

is a tensor containing the derivatives from the failure function in relation to the stress invariants.

DOI: 10.1002/nme

As $h_r(\mathbf{u},\phi) = \max\left\{g_r(\mathbf{u},\phi); -\frac{\alpha_r}{c}\right\}$ where $g_r(\mathbf{u},\phi)$ is given by Equation (22), then if $h_r(\mathbf{u},\phi) = g_r(\mathbf{u},\phi)$

$$\frac{\partial g_r(\mathbf{u},\phi)}{\partial I_1} = \frac{\partial g_r(\mathbf{u},\phi)}{\partial J_3} = 0,$$
$$\frac{\partial g_r(\mathbf{u},\phi)}{\partial J_2} = \frac{3}{2\sigma_{adm}\sigma_r^{vM}}\Psi(H_r(\phi)),$$

and the tensor $\mathbf{A}_r(\mathbf{u},\phi)$ is given by

$$\mathbf{A}_r(\mathbf{u},\phi) = \frac{3}{2\sigma_{adm}\sigma_r^{vM}}\Psi(H_r(\phi))\mathbf{P}^T\mathbf{s}_r(\mathbf{u}).$$

In the case that $h_r(\mathbf{u},\phi) = -\frac{\alpha_r}{c}$, then

$$\frac{\partial h_r(\mathbf{u},\phi)}{\partial I_1} = \frac{\partial h_r(\mathbf{u},\phi)}{\partial J_2} = \frac{\partial h_r(\mathbf{u},\phi)}{\partial J_3} = 0,$$

and the tensor $\mathbf{A}_r(\mathbf{u},\phi)$ is zero.

ACKNOWLEDGEMENTS

The authors would like to thank the CAPES—Coordenação de Aperfeiçoamento de Pessoal de Nível Superior—and CNPq—Conselho Nacional de Desenvolvimento Científico e Tecnológico, Brazil—that provided financial support for this research.

REFERENCES

1. Duysinx P, Bendsøe MP. Topology optimization of continuum structures with local stress constraints. *International Journal for Numerical Methods in Engineering* 1998; **1478**(June 1997):1453–1478.
2. Pereira JT, Fancello EA, Barcellos CS. Topology optimization of continuum structures with material failure constraints. *Structural and Multidisciplinary Optimization* 2004; **26**:50–66.
3. Fancello EA, Pereira JT. Structural topology optimization considering material failure constraints and multiple load conditions. *Latin American Journal of Solids and Structures* 2003; **1**:3–24.
4. Fancello EA. Topology optimization for minimum mass design considering local failure constraints and contact boundary conditions. *Structural and Multidisciplinary Optimization* 2006; **32**:229–240.
5. Allaire G, Jouve F, Maillot H. Topology optimization for minimum stress design with the homogenization method. *Structural and Multidisciplinary Optimization* 2004; **28**:87–98.
6. Bruggi M. On an alternative approach to stress constraints relaxation in topology optimization. *Structural and Multidisciplinary Optimization* January 2008; **36**(2):125–141.
7. Bruggi M, Venini P. A mixed FEM approach to stress-constrained topology optimization. *International Journal for Numerical Methods in Engineering* 2008; **73**(12):1693–1714.
8. Amstutz S, Novotny AA. Topological optimization of structures subject to Von Mises stress constraints. *Structural and Multidisciplinary Optimization* 2010; **41**(3):407–420.
9. Guilherme CEM, Fonseca JSO. Topology optimization of continuum structures with e-relaxed stress constraints. In *Mechanics of Solids in Brazil*, Alves M, da Costa Mattos HS (eds). ABCM: Rio de Janeiro, Brasil, 2007; 239–250.
10. París J, Navarrina F, Colominas I, Casteleiro M. Topology optimization of continuum structures with local and global stress constraints. *Structural and Multidisciplinary Optimization* November 2009; **39**(4):419–437.
11. Xia Q, Shi T, Wang MY. A level set based method for topology optimization of continuum structures with stress constraint. *6th China-Japan-Korea Joint Symposium on Optimization of Structural and Mechanical Systems*, Kyoto, Japan, 2010.
12. Holmberg E, Torstenfelt B, Klarbring A. Stress constrained topology optimization. *Structural and Multidisciplinary Optimization* February 2013; **48**(1):33–47.
13. Farias JMC, Cardoso EL, Muñoz Rojas PA. Topology optimization with stress constraints using superconvergent patch recovery. *3rd International Symposium on Solid Mechanics*, Florianópolis, SC, Brazil, 2011; 175–195.
14. París J, Navarrina F, Colominas I, Casteleiro M. Block aggregation of stress constraints in topology optimization of structures. *Advances in Engineering Software* 2010; **41**(3):433–441.
15. Le C, Norato J, Bruns T, Ha C, Tortorelli D. Stress-based topology optimization for continua. *Structural and Multidisciplinary Optimization* October 2010; **41**(4):605–620.
16. Amstutz S, Novotny AA, de Souza Neto EA. Topological derivative-based topology optimization of structures subject to Drucker–Prager stress constraints. *Computer Methods in Applied Mechanics and Engineering* 2012; **233-236**: 123–136.
17. Sethian JA, Wiegmann A. Structural boundary design via level set and immersed interface methods. *Journal of Computational Physics* 2000; **163**(2):489–528.

DOI: 10.1002/nme

18. Wang MY, Wang XM, Guo DM. A level set method for structural topology optimization. *Computer Methods in Applied Mechanics and Engineering* 2003; **192**:217–224.
19. Allaire G, Jouve F, Toader AM. Structural optimization using sensitivity analysis and a level-set method. *Journal of Computational Physics* 2004; **194**:363–393.
20. Belytschko T, Xiao SP, Parimi C. Topology optimization with implicit functions and regularization. *International Journal for Numerical Methods in Engineering* June 2003; **57**(8):1177–1196.
21. Luo Z, Wang MY, Wang S, Wei P. A level set-based parameterization method for structural shape and topology optimization. *International Journal for Numerical Methods in Engineering* 2008; **76**(1):1–26.
22. Luo J, Luo Z, Chen L, Tong L, Wang MY. A semi-implicit level set method for structural shape and topology optimization. *Journal of Computational Physics* 2008; **227**:5561–5581.
23. Yamada T, Izui K, Nishiwaki S, Takezawa A. A topology optimization method based on the level set method incorporating a fictitious interface energy. *Computer Methods in Applied Mechanics and Engineering* November 2010; **199**(45-48):2876–2891.
24. Yamasaki S, Nishiwaki S, Yamada T, Izui K, Yoshimura M. A structural optimization method based on the level set method using a new geometry-based re-initialization scheme. *International Journal for Numerical Methods in Engineering* 2010; **83**(12):1580–1624.
25. Luo Z, Zhang N, Gao W, Ma H. Structural shape and topology optimization using a meshless Galerkin level set method. *International Journal for Numerical Methods in Engineering* 2011; **90**(3):369–389. DOI: 10.1002/nme.3325.
26. Mohamadian M, Shojaee S. Binary level set method for structural topology optimization with MBO type of projection. *International Journal for Numerical Methods in Engineering* 2012; **89**:658–670. DOI: 10.1002/nme.3260.
27. Sethian JA. *Level Set Method and Fast Marching Methods: Evolving Interfaces in Computational Geometry, Fluid Mechanics, Computer Vision, and Materials Science*. Cambridge University Press: Cambridge, 1999.
28. Osher S, Fedkiw R. *Level Set Methods and Dynamic Implicit Surfaces*, Vol. 57. Springer: New York, 2003.
29. Dijk NP, Maute K, Langelaar M, Keulen F. Level-set methods for structural topology optimization: a review. *Structural and Multidisciplinary Optimization* March 2013; **48**(3):437–472.
30. Allaire G, Jouve F. Minimum stress optimal design with the level set method. *Engineering Analysis with Boundary Elements* November 2008; **32**(11):909–918.
31. James KA, Lee E, Martins JRRA. Stress-based topology optimization using an isoparametric level set method. *Finite Elements in Analysis and Design* October 2012; **58**:20–30.
32. Van Miegroet L, Duysinx P. Stress concentration minimization of 2D filets using X-FEM and level set description. *Structural and Multidisciplinary Optimization* January 2007; **33**(4-5):425–438.
33. Guo X, Zhang WS, Wang MY. Stress-related topology optimization via level set approach. *6th China-Japan-Korea Joint Symposium on Optimization of Structural and Mechanical Systems*, Kyoto, Japan, 2010.
34. Guo X, Zhang WS, Wang MY, Wei P. Stress-related topology optimization via level set approach. *Computer Methods in Applied Mechanics and Engineering* November 2011; **200**(47-48):3439–3452.
35. Xia Q, Shi T, Liu S, Wang MY. A level set solution to the stress-based structural shape and topology optimization. *Computers and Structures* January 2012; **90-91**:55–64.
36. Verbart A, Langelaar M, Dijk NV, Keulen FV. Level set based topology optimization with stress constraints and consistent sensitivity analysis. *53rd AIAA/ASCE/AHS/ASC Structures, Structural Dynamics and Materials Conference*, Honolulu, Hawaii, 2012.
37. Wang MY, Li L. Shape equilibrium constraint: a strategy for stress-constrained structural topology optimization. *Structural and Multidisciplinary Optimization* September 2013; **47**(3):335–352.
38. Suresh K, Takalloozadeh M. Stress-constrained topology optimization: a topological level-set approach. *Structural and Multidisciplinary Optimization* March 2013; **48**(2):295–309.
39. Zhang WS, Guo X, Wang M, Wei P. Optimal topology design of continuum structures with stress concentration alleviation via level set method. *International Journal for Numerical Methods in Engineering* 2013; **93**:942–959.
40. Lee E, James KA, Martins JRRA. Stress-constrained topology optimization with design-dependent loading. *Structural and Multidisciplinary Optimization* 2012; **46**(5):647–661.
41. Osher S, Sethian J. Fronts propagating with curvature-dependent speed: algorithms based on Hamilton–Jacobi formulations. *Journal of Computational Physics* 1988; **79**:12–49.
42. Cheng G, Guo X. ϵ-relaxed approach in structural topology optimization. *Structural Optimization* 1997; **13**:258–266.
43. Bertsekas DP. *Constrained Optimization and Lagrange Multiplier Methods*. Athena Scientific: Belmont, MA, U.S.A., 1996.
44. Martínez JM. Otimização prática usando o Lagrangiano Aumentado. *Technical Report*, IMECC-UNICAMP, 2009.
45. Haug EJ, Choi KK, Komkov V. *Design Sensitivity Analysis of Structural Systems*. Academic Press: Orlando, 1986.
46. Wang MY, Wang X. PDE-driven level sets, shape sensitivity and curvature flow for structural topology optimization. *Computer Modeling in Engineering and Sciences* 2004; **6**:373–395.
47. Wang X, Wang MY, Guo D. Structural shape and topology optimization in a level-set-based framework of region representation. *Structural and Multidisciplinary Optimization* 2004; **27**:1–19.
48. Gournay F. Velocity extension for the level-set method and multiple eigenvalues in shape optimization. *SIAM - Journal on Control and Optimization* 2006; **45**(1):343–367.
49. Dijk NPV, Langelaar M, Keulen FV. Explicit level-set-based topology optimization using an exact Heaviside function and consistent sensitivity analysis. *International Journal for Numerical Methods in Engineering* 2012; **91**((May)):67–97.